

# **MARS EXPLORATION ZONE IDENTIFICATION USING A GEOSPATIAL SUITABILITY MODEL**

by

Minna Adel Rubio, B.Sci Planetary Science, Purdue University

A directed research report submitted to the Department of Geography and Environmental Studies at

Texas State University in partial fulfillment

of the requirements for the degree of

Master of Applied Geography

with a specialization in Geography

December 2023

Committee Members:

Dr. Nathan Currit, Chair

Dr. Justin Wilkinson, Co-Chair

**COPYRIGHT**

by

Minna Adel Rubio

2023

## **FAIR USE AND AUTHOR'S PERMISSION STATEMENT**

### **Fair Use**

This work is protected by the Copyright Laws of the United States (Public Law 94-553, section 107). Consistent with fair use as defined in the Copyright Laws, brief quotations from this material are allowed with proper acknowledgement. Use of this material for financial gain without the author's express written permission is not allowed.

### **Duplication Permission**

As the copyright holder of this work I, Minna Adel Rubio, authorize duplication of this work, in whole or in part, for educational or scholarly purposes only.

## **DEDICATION**

This paper is dedicated to my parents, Anna Laura and Samuel Rubio, who's sacrifices brought me to where I am today.

## **ACKNOWLEDGEMENTS**

Special thanks to Dr. Nathan Currit, Dr. Justin Wilkinson and Dr. Denise Blanchard-Boehm, who's support, insight and guidance made completing this paper possible.

# TABLE OF CONTENTS

LIST OF TABLES.....	vii
LIST OF FIGURES.....	viii
ABSTRACT.....	x
CHAPTERS	
I. INTRODUCTION.....	1
A. Research Objectives.....	2
II. LITERATURE REVIEW.....	3
A. Martian Topography.....	3
B. Evolvable Mars Campaign.....	6
C. The First Landing Site/Exploration For Human Missions To Mars.....	8
D. Mars Geospatial Surface Analysis.....	11
III. METHODS.....	18
A. Data.....	18
B. Methods.....	27
IV. RESULTS.....	36
A. Regional Downselect.....	38
B. In-Depth Look: Region 1.....	38
C. In-Depth Look: Region 2.....	40
D. ICE-WG Requirements.....	41
V. CONCLUSION.....	61
WORKS CITED.....	63

## LIST OF TABLES

Table 1. Relative region scores.....	15
Table 2. Candidate exploration zones in region 1.....	43
Table 3. Candidate exploration zones in region 2.....	48

## LIST OF FIGURES

Figure 1. MOLA data and suitability .....	12
Figure 2. Settlement Favorability Map .....	14
Figure 3. Albedo and Thermal Inertia Suitability .....	31
Figure 4. Ferric Oxide Suitability .....	31
Figure 5. Slope Suitability .....	32
Figure 6. SWIM Suitability .....	33
Figure 7. Suitability Model Result.....	36
Figure 8. Regions with Highest Suitability .....	37
Figure 9. Pathfinder Landing Site .....	39
Figure 10. Sinus Meridiani Region .....	42
Figure 11. Region 1 .....	42
Figure 12. Region 1 Geology .....	45
Figure 13. Terrain Ridges in Region 1 UEU .....	46
Figure 14. Region 2 .....	47
Figure 15. Region 2 Geology .....	49
Figure 16. Kozova Crater .....	50
Figure 17. Region 1 Hydrous Minerals .....	52
Figure 18. Boulder Creating Geologic Features .....	53
Figure 19. Ferric Oxide in Region 1 .....	55
Figure 20. Transformed rasters for Region .....	55
Figure 21. Proposed Region 1 Landing Site .....	56
Figure 22. Landing Site Geologic Features .....	57

Figure 23. Landing Site Albedo .....	58
Figure 24. Landing Site Thermal Inertia .....	59
Figure 25. Landing Site Construction Potential .....	60

## **ABSTRACT**

Mars has been a significant source of scientific interest for decades. Space agencies from around the world have invested time and resources into orbiters, rovers and fly-bys. However, the scientific exploration of the red planet won't stop at remote sensing technologies. The crewed exploration of Mars is one of NASA's major space exploration goals. Using a geospatial suitability model and human geologic interpretation, this project aims to develop a quantitative methodology to identifying landing sites and exploration zones on Mars. A landing site and exploration zone are identified in Sinus Meridiani that meet civil engineering and ISRU parameters identified in NASA literature. Furthermore, this project presents a quantitative, traceable, and adaptable geospatial based methodology that could be adopted in future site selection efforts.

## I. INTRODUCTION

For millennia, scientists have studied planets in our solar system, and over time remote sensing techniques have evolved to where scientists have incredible access to high-quality surface and atmospheric data. These observations have driven research in planetary science and astronomy to new frontiers, uncovering many of the solar system's mysteries.

Because of the planet's proximity, Mars is one of the most well studied planets. Between the National Aeronautics and Space Administration (NASA) and the European Space Agency (ESA), there are two rovers and five orbiters actively studying Mars (NASA 2022). Each mission has collected valuable data that is steadily uncovering Mars' complex geologic, atmospheric, and astro-biological history.

Although remote sensing has created significant headway in Mars research, exploration isn't going to stop at rovers and orbiters. NASA's Mars Architecture Strategy Working Group (MASWG) asserts crewed missions to Mars' surface would be instrumental in furthering humankind's understanding of life's origins and the solar system. Humans are capable of conducting complicated in-situ analyses and are able to precisely handle complex tools (Jakosky et al. 2020). Furthermore, crewed missions offer a level of mobility unseen in robotic missions, expanding science opportunities to "previously inaccessible regions" of the surface (Jakosky et al. 2020).

The federal government has recognized for many years there are strategic, practical and scientific reasons why expanding space exploration to Mars is a priority (NASA 2023). In 2010, the NASA Authorization Act compelled the agency to develop the Space Launch Systems (SLS) rocket and Orion Vehicle, and work towards expanding human exploration beyond low Earth

orbit to the lunar vicinity and eventually to Mars (Bussey et al. 2016) . More recently in 2022, the government directed NASA towards prioritizing the establishment of the Moon to Mars program and the development of propulsion technology for use in future robotic and crewed missions to Mars (US Senate, 117th Congress, H.R. 4346, 2022). To meet these goals, NASA continues to progress through the agency’s mission timelines to provide a workable path from low earth orbit to human exploration of the Mars system (Bussey et al. 2016).

### **A. Research Objectives**

This study will contribute to the greater Mars site selection discourse by using the latest Mars data products and geospatial tools to identify a candidate exploration zone. This project aims to identify an exploration zone and landing site on the Martian surface that is suitable for future crewed missions using geospatial tools from the perspective of NASA’s ISRU and Civil Engineering Working Group (ICE-WG).

## II. LITERATURE REVIEW

### A. Martian Topography

Mars is a terrestrial planet at an average distance of 142 million miles (1.5 astronomical units (AU)) from the sun and 75.6 million miles from Earth. Even though Mars is about half the size of Earth (radius of ~3.4 thousand kilometers), the planet's lack of water bodies results in almost the same land area (Hartmann 2003). Martian days, or sols, are completed in 24.6 hours, slightly longer than an Earth day. One year on Mars is 669.6 sols which is equivalent to 687 Earth days.

Mars is characterized by its prominent hemispheric dichotomy, expressed by the northern hemisphere's relatively smoother plains and the southern hemisphere's heavily cratered highlands (Watters et al. 2007). Topographical measurements from the Mars Orbiter Laser Altimeter (MOLA) show elevation differences between the northern lowlands and southern highlands of greater than 2.5 kilometers, reaching a maximum relief delta of about 6 kilometers in certain areas, a difference comparable to that of the difference between Earth's continents and ocean floors (Watters et al. 2007).

The northern lowlands comprise approximately one third of Mars' surface and center on Mars' north pole (Werner et al. 2011). The northern hemisphere is set apart from its southern counterpart by the area's lower impact crater density and smooth, gently sloping surface (Watters et al. 2007; Werner et al. 2011). The lowlands are composed of several topographic depressions, or basins, that have been infilled with sediments deposited by Late Hesperian outflow channels (Watters et al. 2007). However, there are notable exceptions in the Amazonis and Utopia Planitiae which are thought to have been resurfaced by relatively young volcanic flows from the Elysium and Tharsis volcanic complexes (Watters et al. 2007).

Major geologic regions of the northern lowlands include Amazonis Planitia, Arcadia Planitia, Utopia Planitia, Isidis Planitia, Vastitas Borealis, Acidalia Planitia, Chryse Planitia and Elysium Planitia (Tanaka et al. 2005). Many of these northern regions are locations of successful rover landings. For example, Viking 1 landed at Chryse Planitia, Viking 2 at Utopia Planitia, InSight at Elysium Planitia and Phoenix at Vastitas Borealis. Furthermore, NASA's most advanced rover to date, Perseverance Rover, landed in Jezero Crater in 2021. Jezero Crater sits in the lowland's Isidis Planitia (Tanaka et al. 2005).

The transition zone between the northern and southern hemispheres, called the dichotomy boundary, is geologically complex and known for its mesas, knobs and intervening plains (Smith et al. 1999). Furthermore, there are extreme elevation differences throughout the dichotomy boundary, reaching upwards of 4 kilometers in some regions (Smith et al. 1999). Areas where the elevation differences are especially steep are known as the dichotomy boundary scarp (Smith et al. 1999).

The Tharsis Province is a notable topographic feature because it obscures portions of the dichotomy boundary and dominates the western hemisphere (Watters et al. 2007; Hartmann 2003). Tharsis, centered roughly around the equator, is a large, swelling rise, hypothesized to have resulted from the mass accumulation of volcanic material from previous eruptions (Barlow 2008; Hartmann 2003). It rises approximately 9 kilometers above Mars' mean elevation and is large enough to cover the entire western United States (Hartmann 2003).

Tharsis has an interesting tectonic history of fracturing, faulting, and terrain deformation (Hartmann 2003). Radial fractures observed beginning from the equator to high latitudes (70 N and 70 S degrees) indicate high levels of crustal stress in the area (Hartmann 2003). Tharsis' fracture system expands approximately 8,000 kilometers across Mars' surface (Hartmann 2003).

A result of the area's massive fractures is a complex canyon system called Valles Marineris. The immense canyon extends about 4000 kilometers along Mars' equator and reaches depths of 11 kilometers below surrounding terrain at certain points (Barlow 2008). Initially, the system was a series of narrow fractures that formed throughout Tharsis' volcanic evolution (Hartmann 2003). Eventually, unstable walls collapsed into the canyon's floor and the fractures widened (Hartmann 2003). Furthermore, signs of water erosion near the canyon's east end near Ares Vallis is evidence that water may have played a part in the canyon's formation (Hartmann 2003).

Another striking feature of the Tharsis region are its massive volcanoes. This area of Mars is a hot spot for studying Mars' geologic evolution because of its complex volcanic activity (Ahmad et al. 2021). The area encompassing three of Tharsis' larger shield volcanoes, Arsia Mons, Pavonis Mons and Ascraeus Mons, is commonly referred to as Tharsis Montes (Ahmad et al. 2021). These shield volcanoes range between 350 to 500 kilometers in diameter with caldera summits about 8-17 kilometers higher than the surrounding terrain (Ahmad et al. 2021).

Northwest of Tharsis Montes is the solar system's tallest volcano, Olympus Mons. This 600-kilometer diameter shield volcano rises about 18 kilometers above surrounding terrain, with some features towering 22 kilometers above surrounding terrain. (Hartmann 2003; Ahmad et al. 2021). Olympus Mons is three times higher than Mount Everest and its area would cover the United States' state of Missouri (Hartmann 2003). Research suggests that Olympus Mons' relatively uncratered lava flows indicate the volcano's last eruption was likely within the last 10 MY (Hartmann 2003). For this reason, it's possible that Olympus Mons is not extinct, and may be dormant (Hartmann 2003).

In stark contrast to the smooth northern plains, are Mars' rugged southern highlands.

Mars' southern hemisphere is an immensely cratered landscape featuring large impact basins and extensive valley systems (Rodríguez et al. 2020). This area is home to some of the most ancient terrain on Mars, with the oldest landforms dating from the Noachian period (approximately 4.1-3.7 Ga)(Hartmann 2003; Rodríguez et al. 2020).

The southern highlands are home to Hellas Basin, a prominent topographic feature that dominates much of the southern highlands. Hellas is the largest impact basin on Mars and second largest in the solar system behind the moon's South Pole-Aitken basin (Komatsu et al. 2017). This impact basin is approximately 1700 kilometers in diameter and has a highly eroded rim structure (Hartmann 2003).

Hellas' floor is commonly referred to as "Hellas Planitia," or the low plains of Hellas (Hartmann 2003). The basin floor reaches depths of almost 8,200 kilometers below the surrounding highland, which makes this region the lowest point on Mars (Hartmann 2003). The basin's floor displays complicated sediment layering where inconsistent fluvial processes deposited and eroded material at different rates (Hartmann 2003).

## **B. Evolvable Mars Campaign**

One of NASA's primary exploration goals is to promote scientific innovation, increase international collaboration and benefit humanity by developing sustained human presence in the solar system and on Mars (Williams et al. 2015). A major effort in building a framework to work towards these exploration goals was NASA's Evolvable Mars Campaign (EMC).

EMC was an effort designed to establish a realistic framework geared towards building a sustainable "human presence in the solar system, including a human journey to explore the Mars system" (Williams et al. 2015;Bobskill 2015). EMC built upon previous work and integrated studies to identify the key elements needed to sustain humans on Mars (Hoffman et al. 2016).

The initiative also identified how current programs such as Orion and the Space Launch System (SLS) could be utilized for future exploration needs (Hoffman et al. 2016). Furthermore, EMC emphasized the reuse of systems when appropriate for use in multiple exploration missions (Williams et al. 2015).

EMC utilized a progressive approach to space exploration referred to as a “proving ground” method, in which essential capabilities are validated over several lunar missions (Williams et al. 2015; Crusan et al. 2016). This incremental approach to testing and refining technology will eventually lead to “affordable flight elements and deep space [capabilities],” like crewed missions to Mars’ surface that are relatively Earth independent (Bobskill et al. 2015; Crusan et al. 2016).

The EMC outlined several ground rules and assumptions to guide future mission studies regarding Martian human exploration, one of those being that all mission support and assets were to be concentrated at one location (Bussey et al. 2016). This means that rather than having multiple landing sites across multiple missions, as suggested in other design architectures, EMC missions return to the same chosen landing site multiple times (DRA 5.0 2009; Bussey et al. 2016).

Although EMC is adopting a single landing site approach, the crew will explore an exploration zone (EZ), which is a 100 kilometer radius area where regions of interest (ROI) and the centralized habitat are located (Bussey et al. 2016; Hoffman et al. 2016). The EMC defines ROIs as sites where crew will conduct scientific experimentation, collect samples and develop resources necessary for their sustained presence (Bussey et al. 2016; Hoffman et al. 2016).

The EMC also identified two topographic constraints, one of elevation and a second latitude limitation (Hoffman et al. 2016). Initial latitude constraints are placed at +/- 50 degrees

and elevation is limited to less than +2 km (as measured by the Mars Orbiter Laser Altimeter (MOLA)) (Hoffman et al. 2016). The elevation parameters were constructed around spacecraft ascent and landing capabilities, which prefer mid-high or mid-low elevations (Hoffman et al. 2016). Furthermore, higher latitudes are preferable for water ice that can be used for ISRU and science (Hoffman et al. 2016).

### **C. The First Landing Site/Exploration For Human Missions to Mars**

In 2015, The “First Landing Site/Exploration Zone Workshop for Human Missions to the Surface of Mars” was held, where researchers proposed both exploration zones and regions of interest (ROIs) (Bussey et al. 2016). Members of NASA’s Human Exploration and Operations Mission Directorate and the Science Mission Directorate were tasked with preparing the workshop (Bussey et al. 2016). The purpose of the workshop was to propose landing sites and exploration zones where a crew could live and work on Mars (Bussey et al. 2016).

The steering committee stated that exploration zone/landing site proposers should follow a set of parameters depending on whether the exploration zone was being optimized for science or civil engineering (Bussey et al. 2016). The base requirements for an exploration zone are those listed in Section A of the literature review identified by the EMC including: (a) located between +/- 50 ° latitude. (b) less than +2 km elevation, (c) must feature an area of about 25 km<sup>2</sup> that is relatively free of hazards, and (d) does not contain thick deposits of dust (Bussey et al., 2016).

The In-situ Resource Utilization (ISRU) and Civil Engineering (CE) working group (ICE-WG) was asked to develop a set of requirements for a candidate exploration zone that meets the objectives of NASA’s goal of a sustainable human presence on Mars (Bussey et al.

2016). Therefore, ICE-WG produced three requirements for the workshop and focused the development of their parameters around “just those portions of the EMC dealing with achieving a permanent sustainable presence on the surface of Mars” that limits Earth's reliance (Bussey et al. 2016).

The first listed requirement is that the exploration zone should feature a location with access to material that shows potential produce to be used for water generating purposes (Bussey et al. 2016). The document states the resource can be in the form of ice, ice/regolith mix or hydrated minerals (Bussey et al. 2016). Furthermore, the resource must be as close to the surface as possible and yield significant quantities (>100 MT of water). (Bussey et al. 2016).

Second, the exploration zone should have access to an area that is suitable for infrastructure construction (Bussey et al. 2016). The construction area should feature flat, stable terrain and show the potential to be a source of cobble-sized rocks and/or loose regolith (Bussey et al. 2016).

Third, the exploration should have access to a resource that has the potential to be used as metal or silicon for construction (Bussey et al. 2016). The document lists iron, aluminum and silicon as primary resources of interest (Bussey et al. 2016). Of lesser priority are titanium and magnesium (Bussey et al., 2016).

Additionally, ICE-WG identified two *enhancements*, not requirements, that would benefit an exploration zone (Bussey et al. 2016). First, the exploration zone would be enhanced if there existed additional locations where material with potential to be used as water-generating feedstock within the area (Bussey et al. 2016). This resource should be as close to the surface as possible, but differs from the first requirement such that the quantity the resource should yield is not specified (Bussey et al. 2016).

The second enhancement is that the exploration zone features natural terrain that could be adapted for construction purposes (Bussey et al. 2016). The example given in by Bussey et al. (2016) is that the terrain may act as a body that blocks radiation from the habitat. Listed terrain features that meet this purpose are shallow depressions, narrow (accessible) valleys, and lava tubes (Bussey et al. 2016).

The workshop accepted 45 abstracts that proposed most of the longitude, latitude and elevation parameters identified by EMC (Bussey et al. 2016). Many of the proposed landing sites were concentrated around craters like Gale Crater, Jezero Crater, Gusev Crater and Endeavour Crater (Bussey et al. 2016). The more regional areas where landing sites were proposed were primarily in and around Arabia Terra and Chryse Planitia (Bussey et al. 2016).

Additionally, the workshop solicited feedback from researchers and workshop attendees to gain insight as to how the community would like to continue building on the site selection framework (Bussey et al. 2016). One of the key takeaways included the community acknowledging that at the time of the workshop, there is a substantial amount of data that is useful for site selection that has not been collected yet like radar at shallow depths and require the deployment of new landed instruments or orbiters (Bussey et al. 2016). Also, in this same vein, new data at higher resolutions should be collected, where possible (Bussey et al. 2016).

Another finding of the workshop was that a better understanding of the merits of certain resources such as buried ice deposits, hydrated minerals, hydrated dune fields and recurring slope lineae being used as sources of water was required (Bussey et al. 2016). Furthermore, the researchers acknowledged that more analysis of the currently available data, and new data (when available) is necessary to improve their initial assessments (Bussey et al. 2016).

## D. Mars Geospatial Surface Analysis

In *Planetary Mapping for Landing Sites Selection: The Mars Case Study* by Pajola et al. (2019) shows that GIS is a pivotal resource for site selection because GIS software can integrate both science and engineering requirements. In their study, they evaluate two proposed landing sites. The first site is Simud Vallis, a site proposed earlier by Pajola et al. (2019), for ESA's ExoMars rover. The second site is near Eridania, also previously proposed by one Pajola et al. (2019), for NASA's Mars 2020 mission.

Pajola et al. (2019) produced a series of GIS maps to assist with the terrain analysis. Digital terrain models (DTMs) were used in a GIS environment to identify areas that meet the slope constraints for ESA and NASA's rovers:  $\leq 3.0^\circ$  (2 to 10 km in length),  $\leq 8.6^\circ$  (333 m in length),  $\leq 12.5^\circ$  (7m in length), and  $\leq 15.0^\circ$  (2 m in length) (Pajola et al. 2019).

Engineering constraints stated an acceptable elevation for rover landing sites was  $\leq -2$  km (ESA) and  $\leq +0.5$  km (NASA) based on the Mars Global Surveyor (MGS)-Mars Orbiter Laser Altimeter (MOLA) geoid (Pajola et al. 2019). Therefore, Pajola et al. (2019), used MOLA elevation data to analyze the surface for areas that meet elevation requirements.

To meet other mission ESA and NASA mission requirements Pajala et al. (2019) utilized other datasets such as Mars Global Surveyor (MGS) Thermal Emission Spectrometer (TES) thermal inertia and albedo data to investigate dust coverage (2019). Also, to study the region's rock abundance Pajala et al. (2019) used data from the Viking Infrared Thermal Mapper (IRTM) and, where available, the team used more detailed MGS TES rock abundance maps.

The team overlaid the relevant datasets to identify an area that met each of the criteria (Pajala et al. 2019). An example of one their integrated criteria maps is shown in Figure 1. The

figure shows that the areas not meeting the identified criteria are colorized in red (Pajola et al. 2019). On the other hand, areas that do meet the listed criteria are colorized in green (Pajola et al. 2019). Furthermore, Pajalo et al. (2019) stated that additional maps such as geologic and mineralogical maps should also be overlain during the site selection process to complete science requirements. This is because geologic and mineralogical maps show what scientific benefits could be derived from the landing area (Pajola et al. 2019).

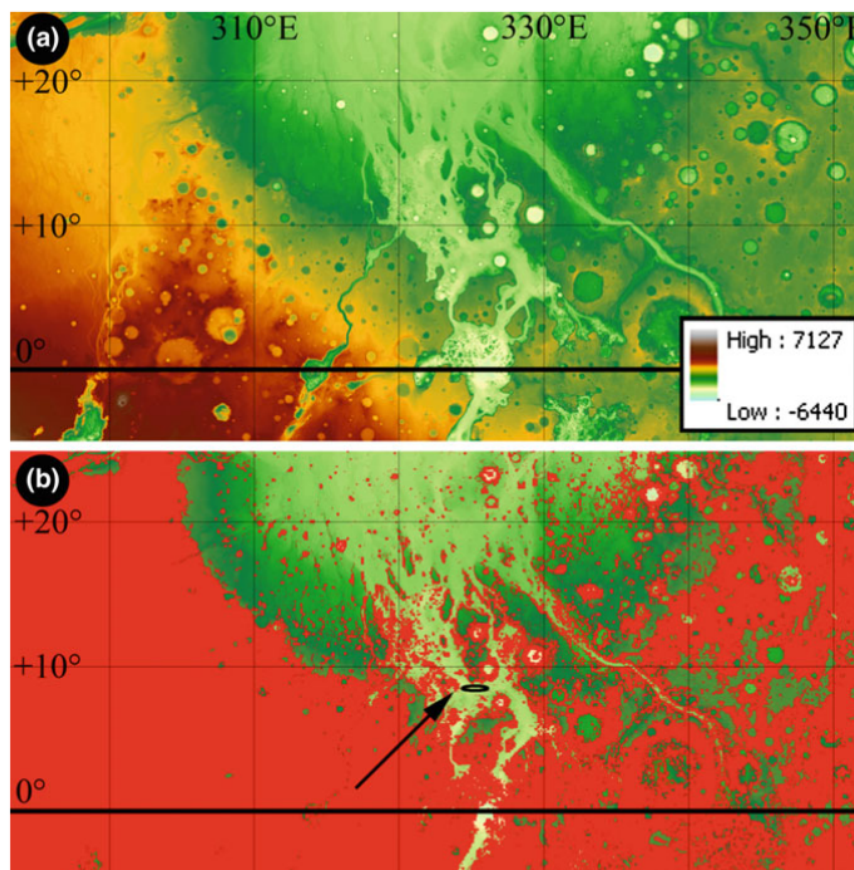


*Figure 1: MOLA data and suitability (a) MOLA-based elevation map (B) Constraint map showing areas that do not meet required criteria (red) and areas that do meet the criteria (green) (Pajola et al. 2019).*

In conclusion, Pajalo et al. (2019) stated that when science and engineering constraints are integrated into one the result is a “complete and consistent landing site proposal” that can be easily evaluated in an objective manner.

In “*Applications of GIS in Analysis of Mars*,” Kuźma et al. (2017) demonstrated the viability of using GIS and remote sensing data to conduct a surface analysis of Mars to identify potential human habitat sites. To achieve this goal the authors used a GIS software and combined the relevant datasets, similar to the method used in Pajalo et al. (2019).

The criteria used in their analysis included temperature (-30° to 30°C), slope, distance from craters (20 km+ in diameter) and sandstorm occurrence (2017). Kuźma et al. (2017) used MOLA’s 460 m digital elevation model (DEM) to create a slope map. The group used MOLA Thermal Emission Spectrometer (TES) data to create a temperature map using unspecified analysis tools.

To parse out “unstable geologic areas” that would not be suitable for a habitat Kuźma et al. (2017) created a feature database that highlighted the location of prospective hazards such as craters, volcanoes and canyons. Then, the team created a 20 km buffer around hazards and dissolved the separate polygons into one polygon. This larger shape represented an “exclusion area” over the Martian surface where a habitat could not be placed.

Lastly, Ruff and Christensen’s 2002 Dust Index Map derived from MOLA TES data was used to find areas with high levels of dust (Kuźma et al. 2017). After all maps were finalized, the products were overlaid to make a single map that visualized areas on a spectrum of “favorable” to “unfavorable” (Kuźma et al. 2017). The team reported that the results of their map (shown in Figure 2) indicate that 43% of Mars’ surface could host a crewed habitat (Kuźma et al. 2017).

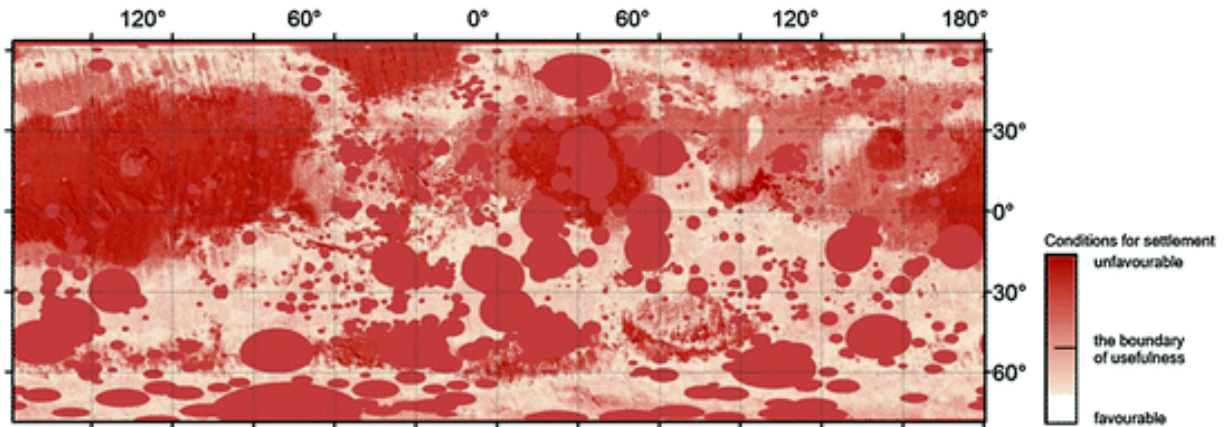


Figure 2: Settlement Favorability Map (Kuźma et al. 2017). The deep red areas are the least favorable while the lighter red toned areas are more favorable.

Kuziakina et al. (2019) conducted a GIS analysis of Mars in “GIS analysis of promising landing sites for manned flight to Mars,” to identify adequate landing sites while prioritizing scientific value and crew safety. Kuziakina et al. (2019) focused their study on 4 areas, which are a subset of 9 landing sites proposed for other missions. The regions are (1) Acidalia Planitia, (2) Schiaparelli Crater, (3) Elysium Planum, and (4) Hellas Plain.

For their analysis, Kuziakina et al. (2019) made use of multiple data remote sensing spacecraft like orbital probes and rovers including MGS, Mars Reconnaissance Orbiter (MRO), Viking-1, Viking-2, and Curiosity rover. Specifically, Kuziakina et al. (2019) used topographic maps, gravitational anomaly maps, surface magnetism maps, an equivalent dose map, maps of volcanoes, day and night temperature maps and fast neutron emission maps. These datasets were used to assess how well the landing sites met the prioritized parameters identified as gravitational anomaly, surface relief, magnetic field strength, absorbed radiation, rock composition, presence of hazards (volcanoes), water presence, and temperature.

The authors scored each proposed region against each other based on a graded set of indicators (daytime temperature, water, rock composition etc.) (Kuziakina et al. 2019). The scores that could be assigned ranged from +2 to -1. The highest rating (+2) means that the area

has a “positive effect” on the indicator (Kuziakina et al. 2019). For example, if the indicator is rock composition and the region has a very low abundance of rocks, that region would receive a score of + 2. At the opposite end, a region found to be extremely rocky would receive the lowest score of -1.

After grading, the region with the highest number of points was deemed the most suitable region for a manned mission. Table 1 shows the teams ranking and total points acquired at each region (Kuziakina et al. 2019). The team’s results indicated that Acidalia Planitia was the most suitable region based on the author’s grading of the datasets (Kuziakina et al., 2019). According to the author’s scale, Acidalia Planitia received 8 out of the maximum 18 points (Kuziakina et al. 2019).

No.	Indicator	Acidalia Planitia	Schiaparelli Crater	Elysium Planum	Hellas Plain
1	Relief (impact on landing difficulty)	2	1	0	-2
2	Gravity anomalies	2	0	-2	1
3	Magnetic field strength	1	2	0	0
4	Absorbed radiation	1	-1	-2	2
5	Rock composition	1	-1	0	2
6	The presence of volcanoes	-2	-2	2	-2
7	Daytime temperature	2	1	1	-2
8	Night temperature	1	-2	-2	-2
9	Water	0	2	2	0
	TOTAL	8	0	-1	-3

*Table 1: Relative region scores. Total scores for each region were reported in the final row of the table (Kuziakina et al. 2017).*

The author of this paper drew several key takeaways from this literature review that played a significant role in the development of this project. The papers discussed in section D “Mars Geospatial Surface Analysis” were successful in their work such that they were able to identify regions or landing sites that met their listed criteria. However, an observation was made that both Pajalo et al. (2019) and Kuźma et al. (2017) created maps that were simple overlays.

Although this method is a fairly standard way to visualize multiple datasets, it does not allow for a truly qualitative comparison of landing sites or regions. For example, the map produced by Kuźma et al. (2017) (shown in Figure 2) appears to reflect habitat favorability but there is no reported numerical pixel data that could be used to compare sites or regions to each other. Furthermore, the only way to assess favorability is to look at the color ramp, which may not appear uniformly across all viewers. This leads to a very subjective way of assessing favorability.

A similar case can be made for Kuziakina et al. (2019), which approached the task a slightly different way. Kuziakina et al. (2019) did not integrate or overlay the maps into a single raster, rather, the team studied the individual datasets at the regional scale. Then, the team assigned a score to each region based on how well they felt the region met their desired criteria. Although the grading scale is a more quantitative method of comparison than the other two studies, it relies solely on the subjective opinion of human interpretation. These two observations inspired the author of this project to investigate methodologies that strayed away from more subjective analysis and attempt to produce a quantitative site comparison.

A positive realization from section “D” is that many of the remote sensing datasets used in the projects can be manipulated in GIS systems that are primarily built for Earth-based analysis. Furthermore, the discussed papers provided a strong foundation for what types of Martian datasets can be used to study specific criteria like elevation, dust cover and temperature.

Furthermore, sections “B” and “C” helped define what NASA leadership considers a good landing site and/or exploration zone. The criteria identified by NASA’s EMC and the ICE-WG that make a successful candidate exploration zone or site can be summarized as a 200 km<sup>2</sup> diameter zone located between +/- 50 ° latitude with an elevation less than + 2 km (Hoffman

et al. 2016; Bussey et al. 2016). Within the exploration zone should exist an area of 25 km<sup>2</sup> with flat, stable terrain that is free of hazards that could be used as a landing site (Hoffman et al. 2016; Bussey et al.2016).

Then, the exploration zone should meet three requirements. The first being that the exploration zone should feature a location with access to materials that could be used to generate water (Bussey et al. 2016). Second, the exploration zone should feature an area that could be used for construction purposes (Bussey et al. 2016). Third, the exploration zone should host a resource that shows the potential to be used as a feedstock for metal or silicon (Bussey et al. 2016).

### **III. DATA AND METHODOLOGY**

#### **A. Data**

##### **Blended Digital Elevation Model (DEM)**

The Mars Orbiter Laser Altimeter (MOLA) is an instrument onboard the Mars Global Surveyor (MGS) spacecraft launched November 1996 by NASA and the Jet Propulsion Laboratory (JPL). MOLA is an optical payload designed with the primary objectives of mapping the Martian surface at a scale appropriate for topographic, geophysical, geological, and atmospheric studies (Smith et al. 2001).

MOLA determines altitude measurements by pulsating an infrared laser at Mars' surface at a rate of 10 hertz (Hz) (Barker, 2023). Once making contact with the surface, the light reflects back towards MOLA and is observed by the instrument's collection mirrors. The time difference between firing the laser and its return is referred to as "time of flight", and it helps scientists calculate MGS' "range" above the terrain within 30 meters (98 feet) (Barker 2023). The measurements collected by MOLA have been used to construct precise topographic maps (Barker 2023).

The European Space Agency's (ESA) orbiter, Mars Express, is a spacecraft launched in 2003 designed to study Mars' atmosphere, surface, subsurface and Moons (ESA 2023). Onboard Mars Express are eight instruments, one of which being the High Resolution Stereo Camera (HRSC). The camera is designed to simultaneously map Mars' topography, morphology, atmospheric phenomena and geologic context (Jauman et al. 2015).

HRSC is a push-broom stereo camera featuring nine charge-coupled devices (CCD) that are configured in parallel to capture , at once, high resolution stereo, multi-color and multi-phase images along the orbiter's track (Jaumann et al. 2015). Over the instrument's lifetime about 90% of Mars has been imaged at a maximum resolution of 10 meters per pixel (with select areas at

about 2 meters per pixel (ESA 2010; Jaumann et al. 2015). In addition, highly precise DEMs have been produced at a maximum of 50 meter grid spacing for over 40% of the surface (Jaumann et al. 2015).

The Mars MGS MOLA-MEX HRSC global DEM is a product derived from blending the 463 mpp DEM with the higher resolution HRSC DEMs (50 mpp) (Ferguson et al. 2017). The HRSC DEMs were reprojected from a sinusoidal projection to simple cylindrical with a chosen cell-size of 200 mpp (Ferguson et al. 2017). The cell-size was chosen as an acceptable compromise between up sampling the MOLA 483 mpp DEM and down sampling HRSC's 50 mpp DEM using a bilinear interpolation method (Ferguson et al. 2017).

Ferguson et al. (2017) state that there are some areas of the blended DEM where blending the two products didn't work well. For this reason, "care should be taken when using for scientific analysis" (Ferguson et al. 2017). The average accuracy is identified at about 100 meters horizontally with an approximate 1 meter radius (Ferguson et al. 2017). Furthermore, the total elevation is +/- 3 meters which is attributed to a global error in the aeroid (+/- 1.8 meters) and regional uncertainties (Ferguson et al. 2017; Nuemann 2002).

The blended DEM was created using HRSC data from 2017 or earlier, and because the HRSC team is continuing to work on all the HRSC DEMs this blended product will eventually be updated (Ferguson et al. 2017). Currently, the HRSC DEMs used in the blended product comprise about 44% of the surface (Ferguson et al. 2017).

For this analysis, the blended DEM was used to derive two products. The first product is a slope raster created using ArcGIS Pro's "Slope" spatial analyst tool which identifies steepness from each cell in the raster (ESRI 2023). Next, an elevation mask was created using the DEM. The mask excluded all elevation values greater than 2 km, which is in accordance with the EMC

exploration zone/landing site requirements (Bussey et al. 2016). The mask was created by simply modifying the raster's symbology such that all values greater than 2 km were set to the color black and acceptable elevations below 2 km were set to transparent.

## **Subsurface Water Ice Map**

The Subsurface Water Ice Mapping (SWIM) is a project developed to support NASA's Mars Exploration Program's efforts to better understand the situation of resources on Mars' surface for future human exploration (Putzig et al. 2022). Not only will subsurface ice deposits be used to sustain a human presence on the surface, but as a resource, water ice can be utilized to refuel spacecraft for return missions (Morgan et al. 2023).

Research shows there are substantial accumulations of water ice in the polar areas (Morgan et al. 2023). Although these polar regions house kilometers-thick ice caps, the high latitudes are not a prime location for landed missions (Morgan et al. 2023). The SWIM team is conducting "global reconnaissance mapping and focused multi-dataset mapping" to characterize water ice abundances from 60°S to 60°N (mid-latitude/equatorial) (Putzig et al. 2022).

Previous water ice mapping relied primarily on analyzing a single data set like neutron maps, thermophysical data, and geomorphic surveys to study ice deposits (Morgan et al. 2022; Putzig et al. 2022). However, SWIM integrates all relevant ice-sensitive datasets into their analysis to search for ice deposits over the entire surface of Mars (Morgan et al. 2022; Putzig et al. 2022). The datasets used for their product include neutron-detected hydrogen (MONS), thermal behavior (TES, THEMIS, and MCS), geomorphology (HiRISE, CTX, HRSC, MOLA) and surface/subsurface radar echoes (SHARAD). Putzig et al. (2022) developed their own technique to extract the most useful information from each dataset.

The group introduced the "SWIM equation" to assess the consistency level of each

dataset with the occurrence of buried water ice (Putzig et al. 2022). For each dataset, the team applied “consistency values” between +1 and -1, the highest number means the data is highly consistent with water ice, 0 means the data gives no indication of the absence or ice, and negative values are highly inconsistent with the presence of water ice in the study area (Putzig et al. 2022). Then the team calculated an overall ice consistency value for each map pixel by adding all the individual consistency values and normalizing by the total number of datasets (Putzig et al. 2022).

For the most current SWIM dataset, the team divided the consistency maps into three depth zones: 0-1 meters, 1-5 meters, and > 5 meters (Putzig et al. 2022). Each zone is weighted based on each of the dataset’s optimal sensing depths (Putzig et al. 2022). For this analysis, the SWIM 0-1 m dataset was used in the suitability model to help identify exploration zones/landing sites that meet ICE-WG requirement 2 detailed in Section C of the literature review.

### **MGS-TES Bolometric Albedo Map**

TES collected global bolometric (visible/near-IR) albedo observations of Mars’ surface (Christensen et al. 2001). Said measurements were used to study the surface material’s properties and changes in the upper most region of the surface (Christensen et al. 2001). In this study, the albedo measurements reported from TES are used to understand Mars’ dust cover, a listed hazard identified by EMC (detailed in Section C).

Dust-free surfaces correlate to regions of Mars that have extremely low albedo measurements (Ruff et al. 2002). According to Christensen et al. 1988, low albedo areas such as Sytris Major are observed to brighten (increase albedo) after dust storms. The same area will then darken (decrease albedo) over time indicating there is a process transporting dust particles from the area (Christensen et al. 1988). TES reports observed albedo values of  $\leq 0.10$  in this

area, therefore, this range of albedo values serves as a proxy for a dust-free or minimally covered area (Christensen et al. 2002).

### **MGS-TES Thermal Inertia Map**

One of TES' objectives was to derive thermal inertia values of Mars' surface at about 3k spatial resolution (Christensen et al. 2001). Thermal inertia is one of the primary factors attributing to the variation of surface temperature and is highly correlated to a material's thermal conductivity (Christensen et al. 2001). Thermal inertia is highly dependent on particle size, rock size, rock abundance and induration degree (Christensen et al. 2001).

Thermal inertia observations can also be used to identify areas that are completely covered by dust (Ruff et al. 2002). Ruff et al. (2002) states that areas of low thermal inertia relate to regions that feature dust layers at least a few centimeters thick. Studies conducted by Presely and Christensen in 1997 show that observations of less than 100 inertia units (IU) have particle size of less than 6 mm. Therefore, in this study, thermal inertia was used to understand the surface's dust cover since it can be said thermal inertia observations of less than 100 IU indicate areas that could be covered by very fine particles (Ruff et al. 2002).

### **OMEGA's Ferric Oxide Map**

Aboard ESA's Mars Express is the Visible and Infrared Mineralogical Mapping Spectrometer (OMEGA) instrument which is designed to map Mars' mineralogical surface characteristics (ESA 2023). One of the products derived from OMEGA's observations is a ferric oxide map which shows the distribution of ferric oxides (also known as Iron (III) oxide) across the surface of Mars (Ody et al. 2012).

Ferric Oxide is the inorganic compound  $\text{Fe}_2\text{O}_3$ , which occurs naturally as the mineral hematite (haematite). As a resource, hematite is economically important since it is a primary feedstock for the steel and iron industries (Kirby 2023). To be specific, iron ore is composed of both hematite and magnetite in varying abundances (Garrison et al. 2001). Since there are a few Hematite adjacent datasets to the author's knowledge, Hematite abundance data was used to identify resources that meet requirement three in Section C.

According to Bandfield's 2002 Hematite detection map derived from TES data, most of the Martian surface is below the Hematite detection limit. Actually, according to Bandfield (2002) there are only two areas on Mars that surpass the detection limit, those two areas being Sinus Meridiani and one pixel in Aram Chaos. Furthermore, Bandfield (2002) asserts that the TES results are logical considering other studies have also found no significant sources of Hematite outside of Sinus Meridiani, Valles Marineris and Arm Chaos.

However, Ody et al. (2012) released the OMEGA ferric oxide map which indicates there is an abundance of ferric oxide material across the surface. Since ferric oxide can be used to indicate the presence of Hematite, this dataset was included in the suitability model. The Ody et al. (2012) map shows that there are other regions in Mars with a relatively high ferric oxide abundance, which contrasts with Bandfield's (2002) Hematite map.

### **OMEGA/CRISM Hydrous Site Map**

Carter et al. (2018) derived a hydrous mineral detection map in shapefile format by combining OMEGA and Compact Reconnaissance Imaging Spectrometer for Mars (CRISM) data. The team performed a "full spectral analysis" to identify and characterize hydrous minerals on Mars. Their work utilized surface reflectance data from the OMEGA and CRISM instruments, which both operate in the visible to near infrared frequency range (Carter et al.

2018). The group only made use of the specific range where spectral features correlate to hydrous minerals (Carter et al. 2018).

Since OMEGA has a lower spatial resolution but greater spatial coverage, this data was used to identify extended exposures of hydrous minerals on a global scale (Carter et al. 2018). The team scanned the entire dataset at all spatial resolutions to find mineral signatures at 1.9 micron (Carter et al. 2018). This corresponded to about 6500 observations, and separated into several clusters where the absorption depth (1.9 microns) was seen above the typical threshold of 2% (Carter et al. 2018). After a manual investigation, Carter et al. (2018) found about 40 new hydrous mineral detections in Terra Sirenum, Thaumasia Planum and Terra Tyrrhena.

A second scan was done in these three regions using OMEGA, though Carter et al. (2018) searched for other absorption bands (~1.9, ~2.2, ~2.3, and ~2.4 microns) and with a lower detection threshold (generally 0-1%). Similar to the first scan, Carter et al. (2018) also conducted a manual verification to discard false positives and other artifacts. The second scan resulted in approximately 400 hydrous mineral exposures identified (Carter et al. 2018).

CRISM has taken observations of almost the entire surface of Mars at a spatial resolution of 100-200 mpp using a relatively low spectral sampling of about 56 nm (Carter et al. 2018). Since this spectral sampling is too low to identify a majority of hydrous minerals, the dataset has rarely been for this work (Carter et al. 2018).

However, Carter et al. (2018) used targeted CRISM observations (higher resolution than 36 mpp) as the major data source for their analysis. Carter et al. (2018) assert that such observations (higher resolution than 36 mpp) are able to identify exposures smaller than 1 km<sup>2</sup>. Further, Carter et al. (2018) clarify that spatial coverage of these types is very low and inhomogenous, and therefore, care should be taken when attempting to derive global

distributions.

Since the CRISM analysis is more complicated, a blind scan of the entire data (like that done with the OMEGA data) was not feasible (Carter et al. 2018). The team analyzed 2220 targeted CRISM observations (out of about 9500 total observations of the data set) based on a set of scientific criteria including regional investigations, targets of opportunity, confirmation/sharpening of a previous OMEGA hydrous mineral detection, confirmation of a detection by other instruments (TES/THEMIS), and 70 other observations were made from CRISM multispectral observations (Carter et al. 2018).

Carter et al. (2018) recognize there is a major bias in the instrument target and their data selection strategies. That being units with no identified geomorphology will be less targeted than those whose geomorphology has been studied (Carter et al. 2018). The authors state that the team analyzed observations from all major units, but most of the targets were concentrated around the southern Noachian highlands, causing a bias in the distribution (Carter et al. 2018).

Furthermore, the study excluded four areas that are known to exhibit major hydrous mineral exposures (Carter et al. 2018). These regions include Sinus Meridiani, Valles Marineris (and chaos), Nili Fossae and northern circum-polar gypsum dune deposits (Carter et al. 2019). These regions have been studied extensively, and Carter et al. (2018) stated their analysis would not contribute to the overall knowledge of those areas.

The authors state since the mineralogy heavily differs from that typically seen in their global study, and the area has been heavily targeted by both OMEGA and CRISM, a high statistical weight would have been placed on those areas and biased the investigations results (Carter et al. 2018). To get ahead of the bias, Carter et al. (2018) included very few CRISM and OMEGA observations in their analysis.

By identifying the individual exposures of hydrous minerals, Carter et al. (2018) inferred a number of actual hydrous mineral exposures. An individual exposure is identified by Carter et al. (2018) by a “group of continuous or loosely continuous pixels which collectively show the same spectral features corresponding to a given hydrous mineral.” When the spatial separation between two groups of pixels was great enough, they were considered two separate sites (Carter et al. 2018).

Even if there were multiple mineral species detected within a group of pixels, Carter et al. (2018) still considered the exposure as one detection, and not two or multiple. This was done because Carter et al. (2018) assert that they found it’s likely that minerals are genetically connected and belong to a single site despite being different minerals. Overlapping detections made by CRISM and OMEGA also only count as one exposure (Carter et al. 2018). Without grouping, Carter et al. (2018) state that they identified about 10,000 individual hydrous mineral exposures using their methods. The resulting map including grouped exposures results in a total of 1,230 sites where 260 were observed only with OMEGA, 800 solely with CRISM, and 170 sites were detected by CRISM and OMEGA (Carter et al. 2018). For this project,

For this project, the OMEGA/CRISM hydrous mineral exposure map was used to form individual landing ellipses. This was done to ensure that the exploration zone met requirement one defined by ICE-WG in Section C of the literature review that states hydrous minerals can be used as a resource for water generating ISRU processes (Bussey et al. 2016)

### **MRO Context Camera (CTX)**

The CTX, led by Malin Space Science Systems (MSSS), captures images of Mars at an altitude of about 250 miles (400 kilometers) (NASA, 2023). The camera, currently in orbit, was designed to take big-picture images of the surrounding terrain to support observations captured

by HiRISE and CRISM. In addition, the camera is used to monitor terrain changes and captures stereo pairs of regions of critical scientific interest (MSSS, 2023). Each swath spans about 19 miles (30 kilometers), and the camera's resolution is 6 mpp (NASA, 2023). At the time of this document, MSSS reports that CTX has imaged more than 50% of Mars (2023).

## **B. Methods**

This study will conduct a multilevel suitability analysis on Mars' surface to identify regions that meet the parameters outlined by the EMC and ICE-WG. The first level analysis will use ArcGIS Pro's suitability model to produce a suitability raster. This data, coupled with a latitude mask that excludes areas outside of +/- 50 degrees N/S -will help narrow focus to regions where viable exploration zones could exist.

The level 1 analysis of this project assists in quickly prioritizing which areas of the surface are more suitable, but utilizes more coarse datasets. For this reason, the level 2 portion of the project will focus on using higher resolution imagery to study the geology and ensure it meets hazard requirements. The analysis will result in the identification of a plausible landing site/exploration zone by integrating higher resolution datasets, a suitability model and resource/geologic maps.

### **Image Processing**

For this project, some image processing was required to translate the data into GIS ready products. To achieve this, the author used the Integrated Software for Imagers and Spectrometers (ISIS) and the Geospatial Data Abstraction Library (GDAL). ISIS is a free-to-use and open-source software (FOSS) created by the United States Geological Survey (USGS)

Astrogeology Center. The software was developed for NASA and the greater planetary science community as a fundamental tool for processing data from an archival state into a format that is analysis-ready (USGS Astrogeology 2022).

Image processing capabilities include adjusting contrast, stretch, image algebra, filters, and statistical analysis. One of the software's major draw points is that it features the unique ability to correctly cartographically place data on non-Earth planetary bodies (USGS Astrogeology 2022). This means that the data can be used to produce other mapping products such as topographic or cartographic maps, DEMs, and more. For these reasons, ISIS is a valuable tool in supporting planetary missions that require the use of non-Earth planetary data (USGS Astrogeology 2022).

GDAL is an open-source software developed by the Open Source Geospatial Foundation. The software is a vector and raster translator library that comes with a diverse set of command line options that offer tools for data translation and processing (Warmerdam 2008).

## **ArcGIS Pro Suitability Modeling**

A suitability model is used to identify areas of interest within a defined region that satisfy a specific set of parameters and are commonly used as a tool to assess habitability and site selection. This project used ArcGIS Pro's in-suite suitability model to create a suitability map to assist in identifying exploration zones that meet requirements outlined by NASA's ICE-WG.

ArcGIS Pro's "Suitability Modeler" is available through the software's Spatial Analyst extension license. The tool allows the user to create a suitability model in an integrated framework that then produces a suitability raster for analysis (ESRI 2023). The process of creating a suitability model is an iterative process composed of refining model parameters,

scaling factors and their relative weights to determine site suitability (ESRI 2023).

This project followed the standardized workflow defined by ESRI (ArcGIS Pro's developer). The software's documentation describes four basic steps: acquire and prepare data, transform raster values of each criterion to preferred suitability scale, weight/combine criteria, locate suitable areas (ESRI 2023).

### **Data Normalization/Transformation**

After acquiring and preparing the desired data, the individual rasters must be normalized (transformed) to a common scale before mathematically combining into a final suitability raster. If the rasters aren't normalized to the same scale before combining them the resulting raster will have meaningless values (ESRI 2023). For this project, the rasters that were transformed are described in the data section of chapter 3, "Data and Methodology."

The integrated suitability modeler in ArcGIS Pro offers a variety of normalization scales. There is not one specific scale that is better than the other, rather it is solely based on preference. In this project, a suitability scale of 1 to 10 is applied to each raster during the data transformation phase, where 1 is least suitable and 10 is most suitable.

It's important to note that the transformations defined in the upcoming sub-sections were extensively iterated upon by the author. No where in the literature available to the author at the time of this project, including documents where architecture or parameters are defined, is a preference (weighting) given to any of the listed parameters (besides some being requirements and some being considered enhancements). For this reason, significant thought and testing was done until reaching a result that seemed reasonable and would result in a safe exploration zone.

### **Transforming Thermal Inertia and Albedo Values**

The thermal inertia and albedo maps were both transformed to a scale of 1 to 10 to

reflect the requirements identified by EMC and ICE-WG. According to Bussey et al. (2016), an exploration zone should not contain “thick deposits of fine-grained dust” because it is an identified hazard. For example, the exploration zone should not be an area with very low thermal inertia and high albedo (Bussey et al. 2016).

According to Ruff et al. (2016), thermal inertia values less than 100 IU correlate to areas where fine -grained dust is at least several centimeters thick (2016). As seen in Figure 3, the map’s original values were transformed such that all values less than 100 IU are assigned the lowest suitability value (1) because that means there likely exists a layer of fine grained dust several centimeters in thickness (Ruff et al. 2016). In contrast, values greater than 100 IU are assigned increasingly greater suitability values ranging from 2-10 because it is unlikely that a relatively thick layer of dust might exist there (Ruff et al. 2016).

Scoring the thermal inertia values on a gradient of suitability values rather than assigning all other values greater than 100 IU the highest value (10) produced better results. This is because there are areas of intermediate to light dust coverage according to the non-transformed thermal inertia map. The highest thermal inertia values are associated with bedrock, while the intermediate values are much harder to interpret because they could be caused by “mixtures of dust and coarse particles” (Ruff et al. 2016). Therefore, it was best that the suitability model also reflect the coverage discrepancies between the highest and intermediate values of thermal inertia.

According to Ruff et al. (2016), albedo values less than or equal .10 correlate to dust free areas. For this reason, albedo values less than or equal to .10 were assigned the highest suitability value of 10 because it’s likely these areas are dust-free (Ruff et al. 2016). Similar to the rationale behind the suitability values detailed for the thermal inertia map, values greater than .10 were assigned lower suitability scores ranging from (8-1).

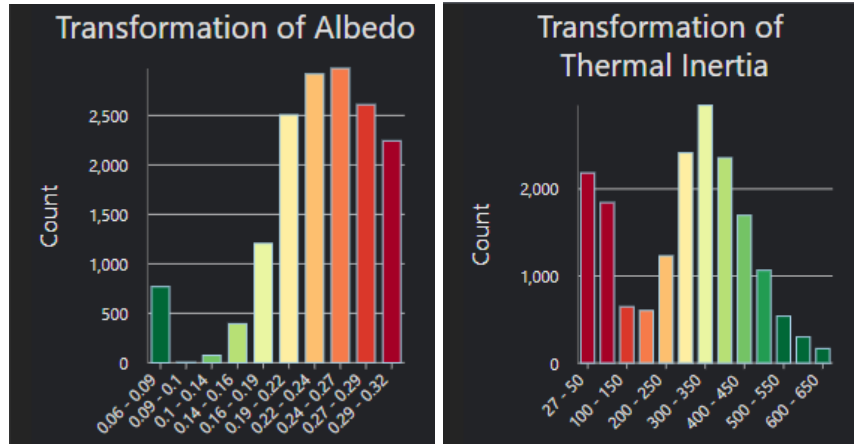


Figure 3: Albedo and Thermal Inertia Suitability. Histograms visualizing how the albedo (left image) and thermal inertia (right image) were transformed on the suitability scale. Redder values indicate lower suitability (lowest suitability score = 1), greener values indicate more suitable (highest suitability score = 10).

### Transforming Ferric Oxide Values

The Mars Express ferric oxide map values were transformed in a way that prioritizes high abundance values. Since there wasn't a specific range requirement outlined in the Bussey et al. (2016) document, a continuous function transform was applied rather than a range of classes transformation (like that applied to the albedo and thermal inertia rasters). This type of transform is most commonly applied to continuous datasets, like the ferric oxide map, that do not need to be transformed with specific ranges in mind. Figure 4 shows the ferric oxide suitability values produced by the transformation.

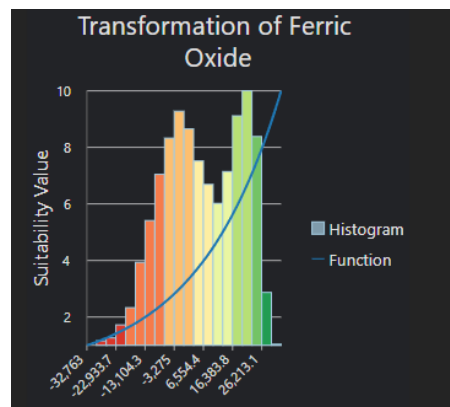
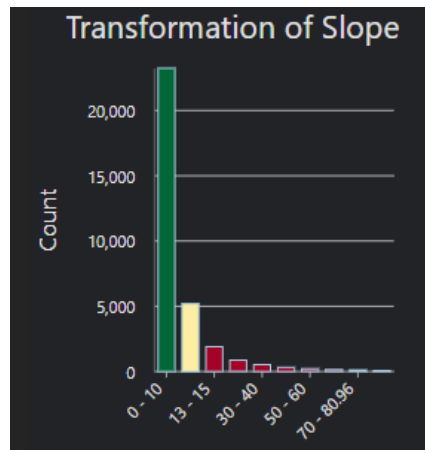


Figure 4: Ferric Oxide Suitability. Continuous transform plot visualizing how the values were transformed on the suitability scale. More red values indicate less suitability. More green values indicate higher suitability.

## Transforming Slope Values

Suitable slope values are identified to be about 10 degrees (Ruff et al. 2016). Therefore, all values less than 10 degrees are assigned a suitability value of 10 using the “range of classes” transformation option (Figure 5). However, to compensate for the total elevation uncertainty (+/- 3 m) detailed by the data’s production team, slope values between 10-13 degrees were assigned a suitability value of 5 (Ferguson et al. 2017). All other values are assigned a suitability value of 1.



*Figure 5: Slope Suitability. Histogram visualizing how the slope values were transformed on the suitability scale. Red values indicate suitability value of 1. Green values indicate suitability value of 10. Yellow values indicate suitability value of 5.*

## Transforming SWIM Values

The SWIM dataset was assigned suitability values based on the interpretation detailed by Putzig et al. 2022. The SWIM data team states that a value of +1 is highly correlated to the presence of ice (Putzig et al. 2022). Therefore, all values equal to +1 were assigned a suitability value of 10 using the “range of classes” transformation method. Putzig et al. (2002) state that map values of 0 mean that there is no indication of the presence or absence of ice. Due to the ambiguity, data values of 0 are assigned a suitability score of 5 since those areas may or may not have ice present (Putzig et al. 2022). The authors list data values equal to -1 are wholly inconsistent with the presence of ice (Putzig et al. 2022). For this reason, those values were

assigned a suitability score of 1 (least suitable). The intermediate values between -1 to 0 and 0 to + 1 are assigned suitability scores between 2 to 4 and 6-9 respectively (Figure 6).

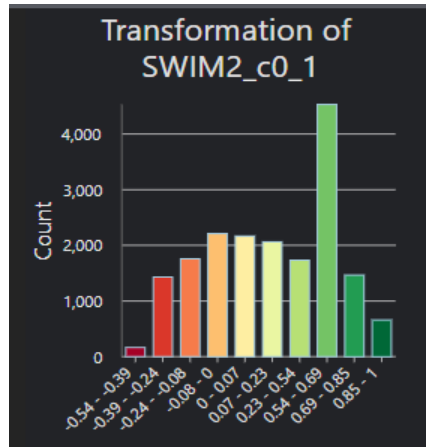


Figure 6: SWIM Suitability. Histograms visualizing how the SWIM data was transformed on the suitability scale. Redder values indicate lower suitability (lowest suitability score = 1), greener values indicate more suitable (highest suitability score = 10).

## Raster Weighting

After transforming the suitability model criteria, the last step before mathematically combining the data is to apply a raster weighting. By default, the model criteria are assigned equal weighting. This implies none of the input parameters are more important than the next. It's true that parameters outlined by EMC and ICE-WG are listed as *requirements*, and those requirements are not graded in preference relative to each other.

However, it's clear that some of the datasets included in the model (like thermal inertia and albedo) contribute more to the identification of hazards than others. For this reason, it was decided that a multiplier or percent increase should be applied to reflect the importance of those datasets that increase the likelihood of preserving spacecraft and crew safety. It's important to note that these weights are being applied with no guidance from mission planning/site selection literature since this information is not publicly available to the author at the time of this project.

Bussey et al. (2016), state that fine-grained dust is a hazard, and the exploration zone/landing site should be relatively free of said hazard. According to Ruff et al. (2016), thermal inertia is an appropriate proxy in identifying fine-grained dust. In the same vein, very low albedo values can be used to identify areas that would be considered dust-free or of low dust coverage. Since both rasters help to discern suitable areas based on a high priority requirement they were assigned the highest multiplier weighted at 2x.

Bussey et al. states exploration zones should have slopes of less than 10 degrees (2016). Since slope is another hazard that contributes to spacecraft and crew safety it was weighted more than some of the other rasters. However, because a vast majority of the terrain in the searchable area (+/- 50° latitude) is relatively flat it was seen that applying the same multiplier as albedo/thermal inertia (2x) seemed to counteract the effectiveness in identifying dust-coverage. For this reason, the slope raster was weighted less than both the albedo and thermal inertia rasters to preserve how well those rasters contributed to hazard detection and instead was given a slightly lower multiplier of 1.5x.

The ISRU and CE exploration zone requirements outlined in the Bussey et al. (2016) document state that it is a requirement for the area to exhibit the potential to have a resource that may be used as a metal or silicon feedstock for construction purposes. Interestingly, the areas with highest iron oxide (most suitable) correlate to the areas that are least suitable for both albedo and thermal inertia. Although the ferric oxide map helps in meeting a list requirement, applying an equal or higher multiplier than thermal inertia and albedo was also found to counteract the effectiveness of identifying hazards that could affect crew and spacecraft safety.

When testing different multipliers for this dataset, it was found that a multiplier of 1.25x didn't have an effect on the overall suitability, but 1.75x seemed to bias the result too much from

thermal inertia/albedo. However, a final multiplier weight of 1.5x was settled on because it was able to still make an effect on the suitability map result without being overpowering, but also wasn't so low that the dataset was being washed out from the model.

The SWIM data, which identifies subsurface water ice up to 1 meter below the surface, was weighted at 1.25x. This multiplier value was found appropriate because of the fact it is going to be coupled with ESA's hydrous mineral map and does not contribute to hazard detection. It would bias the overall results of the study to prefer areas that meet only one of the Bussey et al. (2016) requirements to equally weight the SWIM dataset to slope and ferric oxide while also using the hydrous mineral locations to create exploration zones.

## IV. RESULTS

The analysis results are a suitability raster (Figure 7) with a combined maximum suitability score of 62 (perfect suitability). For a pixel to have perfect suitability, the pixel would have received the highest suitability score in every transformed input. According to the raster statistics available in ArcGIS Pro the minimum suitability value is 14 (not suitable).

Furthermore, the statistics show the mean suitability of the analysis area is 41.75 (moderate suitability).

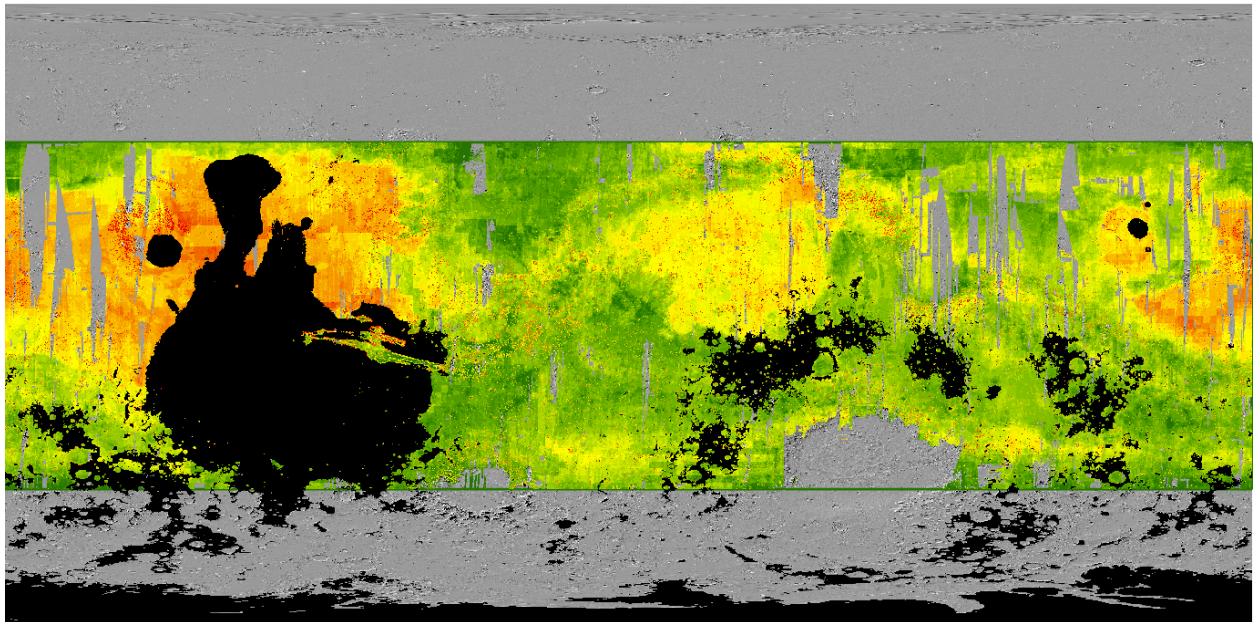


*Figure 7: Resulting suitability map produced from the model. A 2 km elevation mask is placed over the raster (black). The more red, the less suitable. The greener, the more suitable. Transparent areas have no value.*

The suitability map bounds, shown in Figure 7, does not extend higher or lower than +/- 50° latitude because of the parameters outlined by the EMC (Bussey et al. 2016). Also, Figure 7 depicts how there are expansive regions of the surface that have medium-high (40-50 score) to high suitability (50-62 score) rather than only small enclaves of suitability. Furthermore, Figure 7 shows how the low suitability (30-40 score) to unsuitable (14-30 score) areas are isolated to two sizable chunks of the map identifiable by its dark orange-red hued coloration.

Figure 8 shows regions that very high to perfect suitability (50-62 score) areas exist within Chryse Planitia, Arabia Terra and near Valles Marineris. Notable sites of interest in these highly suitable areas are the Opportunity Rover landing site (Arabia Terra) and the Pathfinder landing site (Chryse Planitia). A major takeaway from Figure 8 is that even though an area may have received a suitability score between 50-62 ( high-perfect suitability) it could have been excluded from consideration because it violated the EMC elevation requirement. In fact, some of the highest suitable areas did not end up having an exploration zone placed in the area for other reasons that will be discussed in future sections.

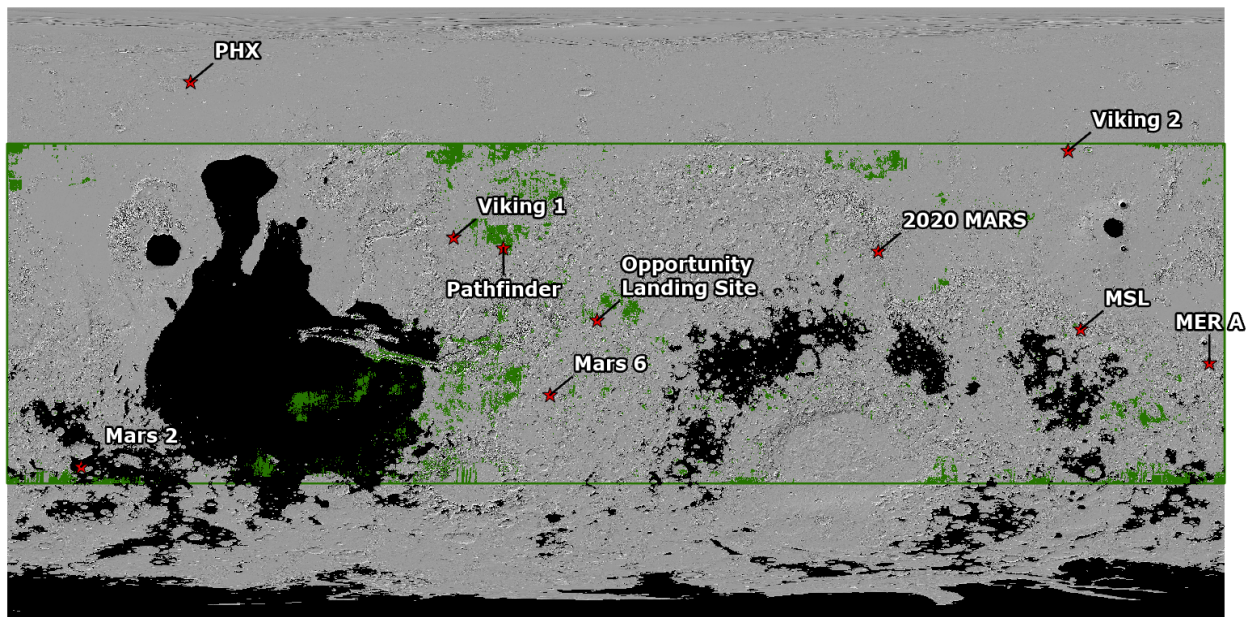


*Figure 8: Regions with Highest Suitability. This map shows the areas of Mars that received the highest suitability scores (50-60) in dark green. Locations where exploration zones could not be placed intersect with the black mask.*

## **A. Regional Downselect**

### **Level 1: Phase 1**

At the start of the first phase, the hydrous mineral distribution map was used to form exploration zones. This decision ensures that the stated requirement of the landing site existing within an exploration zone that features at least one location where potentially useful water-generating resources are accessible is addressed (Bussey et al. 2016). Furthermore, it's a simple way of narrowing down the total analysis area while also meeting stated requirements.

The exploration zones were created using ArcGIS Pro's "buffer" tool. This tool accepts a point file, like the hydrous mineral map, and generates a circular buffer of user defined diameter (in this case 200 km) centered on each point. At this stage, about 1,200 200-km diameter exploration zones were identified within the +/- 50° analysis area based on only the presence of hydrous minerals. Since the hydrous mineral detections are relatively dense, many of the exploration zones overlapped. This resulted in some exploration zones having many instances of hydrous mineral detections, which only positively contributes to addressing the ICE-WG water-generating resource requirement.

The exploration zones being centered on hydrous mineral detections is the main reason why some of the higher suitable areas (like in Chryse Planitia) did not move further into the landing site selection process. For example, the Pathfinder landing site in south Chryse Planitia scored relatively high on the suitability scale, but there were no hydrous mineral detections in that area. There are a few detections scattered more than approximately 430 km grid west of Pathfinder (near the Viking 1 landing site), but the exploration zones generated there did not overlap with those high suitability areas. The suitability score near the Viking 1 landing site (grid north west of Pathfinder) ranges from about 45 (medium high suitability) at the most to about 37

(low suitability).

Furthermore, for the highly suitable Pathfinder area specifically, the lack of a hydrous mineral detection was significantly damaging. Since the area scored so high on the suitability scale, the author considered still moving forward with a candidate exploration zone by manually placing one centered near Pathfinder's landing site. However, upon further inspection of both the original SWIM data and transformed SWIM data, it was found that the Pathfinder area shows very little evidence of subsurface water ice (Putzig et al. 2022).

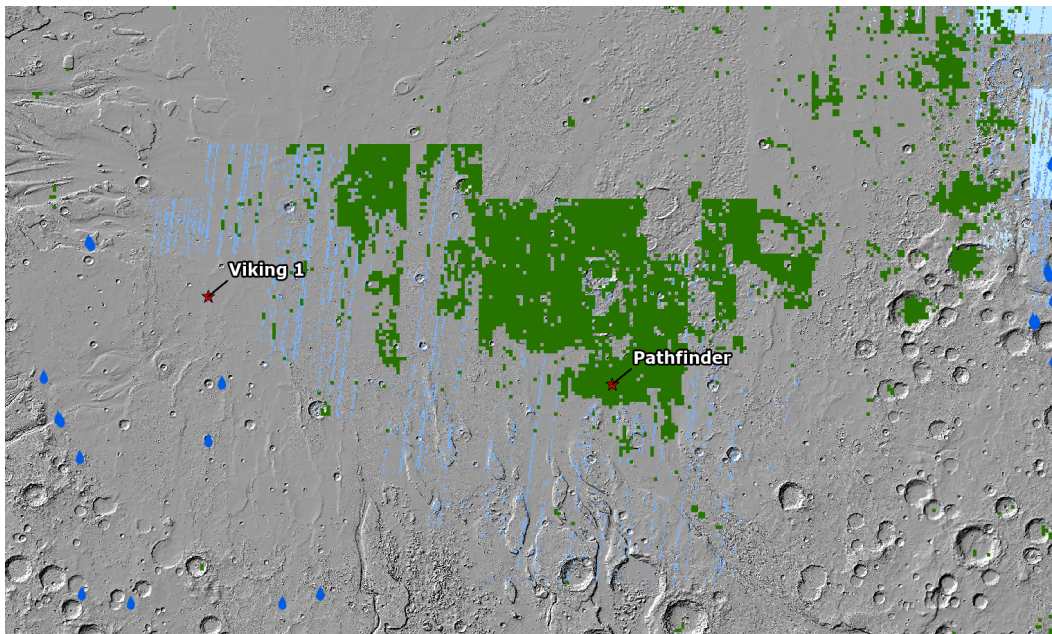


*Figure 9: Pathfinder Landing Site. Map illustrating how the highly suitable (dark green area) Pathfinder landing site area shows little prospect of satisfying the water-generating resource requirement by ICE-WG. There are no hydrous mineral detections (blue droplets) in the area, nor is there strong evidence from the SWIM dataset (light blue streaks) that subsurface water-ice exists in that area.*

It so happened that since the SWIM dataset was weighted lower than all other criteria, it did not have much of an effect on the area's suitability because it scored so highly on all other higher weighted criteria. However, since there are no hydrous mineral detections, and the SWIM data indicates there is little evidence of subsurface water-ice it was determined that there was little prospect of an exploration zone placed in that area satisfying the water-generating ISRU

requirement identified by ICE-WG (Figure 9).

Although there were more than 1,000 candidate exploration zones generated, not all of them were in accordance with baseline EMC requirements. During this phase of strict down-select, all exploration zones that violated the elevation parameter (less than 2 km in elevation) were removed from exploration zone/landing site candidacy. Because there isn't any clarifying literature that specifies how much of an exploration zone can be higher than 2 km this termination was done even if there were some parts of the exploration zone that did meet the elevation requirement.

Also, exploration zones were removed from candidacy if it violated the latitude restrictions. This includes any exploration zone where any part of its extent extends outside of the latitude boundary. Also, buffers that intersect areas of "no data", meaning areas where there are data gaps and the suitability model could not be completed, were removed from exploration zone consideration. After this first phase of down-select, the exploration zones options were whittled from more than 1,200 candidate exploration zones to 624.

## **Level 1: Phase 2**

To further refine candidacy, zonal statistics was used to compare the suitability values amongst the exploration zones. Zonal statistics is a tool in ArcGIS Pro that allows the user to calculate the cell value statistics across a raster within a defined zone (ESRI 2023). ArcGIS Pro has two versions of this tool available, Zonal Statistics and Zonal Statistics as Table, the latter of the duo was used in this project.

The result of this tool is a table that displays the statistics values as defined by the input zones. In this case, the predefined zones are the 200 km exploration zones and the raster from which the statistics are being calculated is the suitability raster. There is one record per zone, and

overlapping zones do not affect the statistics.

Zonal Statistics provides multiple statistical values including mean, median, min and max suitability values. The top 20 exploration zones based on mean suitability were selected for further analysis and separated into two groups of 10. Region 1 (R1) contains the top 10 exploration zones and region 2 (R2) contains the 10 subsequent candidate exploration zones.

### **Geologic Summary of Region 1 and 2**

Region 1 and region 2 are in an area of Mars called Sinus Meridiani, located between the northern lowlands and southern highlands (Wilkinson et al. 2023). As seen in the Edgett (2005) map (Figure 10) Sinus Meridiani is split into four regions: north, east, west, and south. The southern and eastern sections of the region differ from the northern and central areas because of their more cratered surfaces (Edgett 2005). Northern Sinus Meridiani is characterized by the presence of layered, light-toned, rocky outcrops (Edgett 2005). Central Sinus Meridiani is known for its relatively crater-free and flat topography, as well as its association with the presence of hematite (Edgett 2005). Specifically, region 1 and 2 are in the transitional area between eastern and southern Sinus Meridiani.

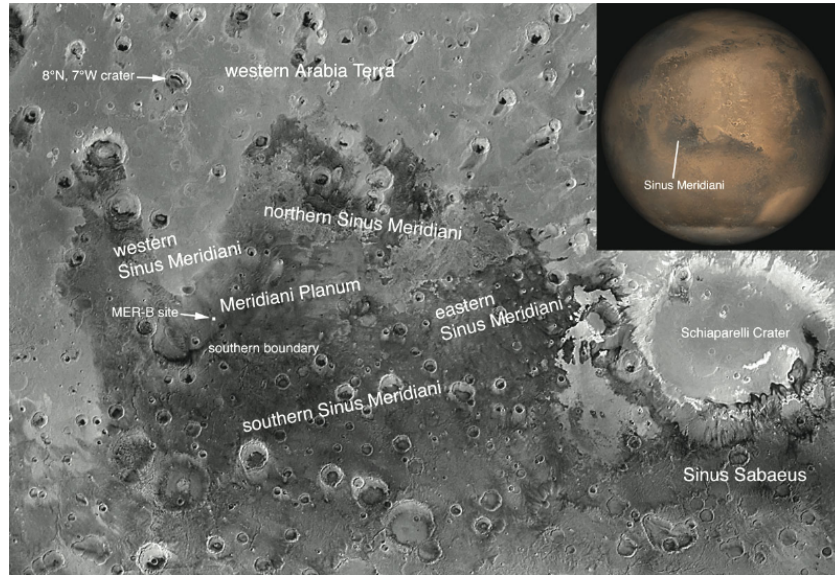


Figure 10: Sinus Meridiani Region. Source: Edgett 2005

## B. In-Depth Look: Region 1

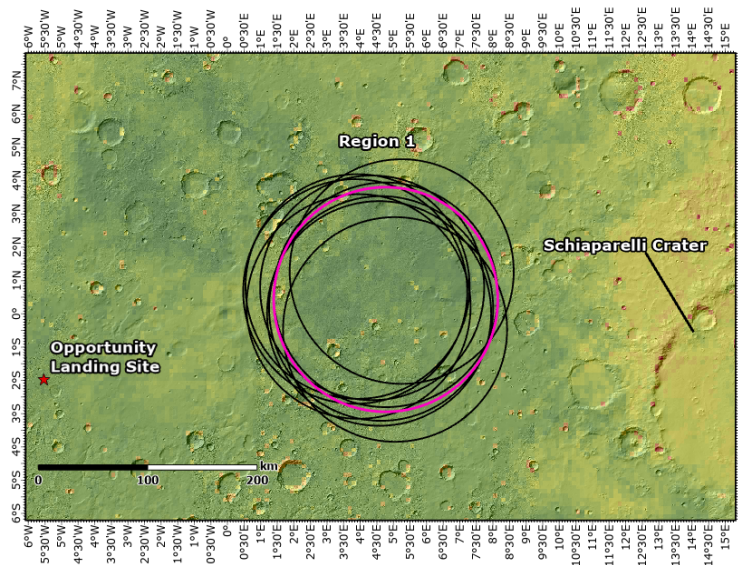


Figure 11: Region 1. Exploration zone 684, with the highest suitability score, is colored in magenta. The final suitability raster, with transparency, is overlaying the MGS shaded relief (Ferguson et al. 2017; own study).

Region 1 is a group of 10 candidate exploration zones that had the highest mean suitability score derived from the zonal statistics analysis in level 1: phase 2 outlined in the previous section. As mentioned, region 1 is in the bordering region between northern and eastern

Sinus Meridiani. Figure 11 shows that region 1 lies west/north-west of Schiaparelli Crater and north-east of the Opportunity Rover landing site.

The candidate exploration zone with the highest suitability is exploration zone 684 (magenta colored exploration zone in Figure 11). Zonal statistics showed that exploration zone 684 has a mean suitability score of about 50.17 (very high suitability). The center of exploration zone 684 is about 325 km east of the Opportunity Rover landing site (pictured in Figure 11) in Meridiani Planum. Out of the top 10 (Table 2), zonal statistics showed that exploration zone 694 has the lowest mean suitability inside the region at a score of 49 (medium-high suitability). Overall, many of the candidate exploration zones within region 1 border just below the very high -perfect suitability range (50-62 score) with only 4 candidate exploration zones falling lower than a score of 50, and by not much.

Exploration Zone ID	Exploration Zone Rank	x (°)	y (°)	Suitability Score
680	7	5.25	1.29	49.93494
682	5	5.05	-0.45	50.0631
684	1	4.77	0.45	50.16925
686	2	4.77	0.59	50.14348
688	3	4.63	0.18	50.12451
690	4	4.57	0.03	50.12451
692	6	4.36	0.8	50.0364
694	10	3.95	0.24	49
1543	8	3.92	0.84	49.90626
1545	9	3.85	0.69	49.90626

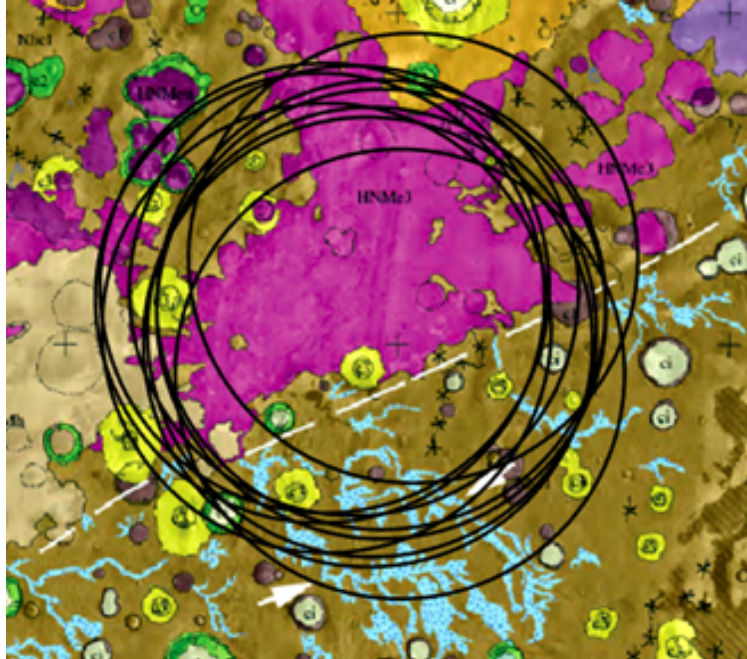
*Table 2: Candidate exploration zones in region 1. Listed are the exploration zone coordinate in decimal degrees, exploration zone rank, suitability score and exploration zone ID.*

Figure 12 shows that region 1 straddles the ridge-forming unit (RFU) and more ancient

Noachian terrain. Units that are north of the dashed line in Figure 12 comprise the RFU, while units below the white dashed line are more ancient terrain (Hynek et al. 2017; Wilkinson et al. 2023). A unit that comprises the ancient terrain is called the Subdued Crater Unit (SCU) (medium brown colored unit within region 1 in Figure 12) (Hynek et al. 2017; Wilkinson et al. 2023).

SCU features more widespread and relatively less rugged terrain than some of the other surrounding units (Hynek et al. 2017). Furthermore, this unit generally shows low albedo values and intermediate thermal inertia (Hynek et al. 2017). Also, craters with high degradation states, subdued rims and infilled floors are common in the SCU (Hynek et al. 2017). There are also wrinkle ridges, scarps and integrated valley networks through the entire unit (Hynek et al. 2017; Wilkinson et al. 2023).

North of the dashed-line is the RFU, which features more rugged, etched terrain (Wilkinson et al. 2023). The RFU terrain is more rough, with widespread raised ridges (Wilkinson et al. 2023). The Upper Etched Unit (UEU) (dark magenta colored areas within region 1 in Figure 12) is above the dashed line and is a RFU (Hynek et al. 2017; Wilkinson et al. 2023). UEU features a distinctly high thermal inertia and generally high albedo with more rugged terrain than surrounding geologic units (Hynek et al. 2017).



*Figure 12: Region 1 Geology. Overlain with the candidate exploration zones in region 1. Dark magenta color represents the UEU, medium brown tan color represents the SCU. (Hynek et al. 2017 map edited by Wilkinson et al. 2023.)*

CTX imagery collected for region 1 supports the assertions by Hynek et al. (2017) and Wilkinson et al. (2023). In some portions of region 1 where SCU is dominant, there exist vast swaths of relatively smooth intercrater plains interwoven amongst the ridges and craters where a 25 km<sup>2</sup> landing site could be placed. There are also many large craters of diverse diameters throughout region 1. Many of the smaller craters (less than 1km) have fairly degraded rims or have been infilled to an extent. These intercrater plains are mantled with a low-albedo material similar to that found near the Opportunity landing site (Edgett 2005).

In region 1 where the UEU are dominant (dark magenta color in Figure 12), there are extensive networks of diverse ridges and the terrain is more rugged and less mantled compared to the SCU surface (Figure 13). The crater population in this unit seems less compared to the SCU, however, the craters that are intact have more pronounced rims.

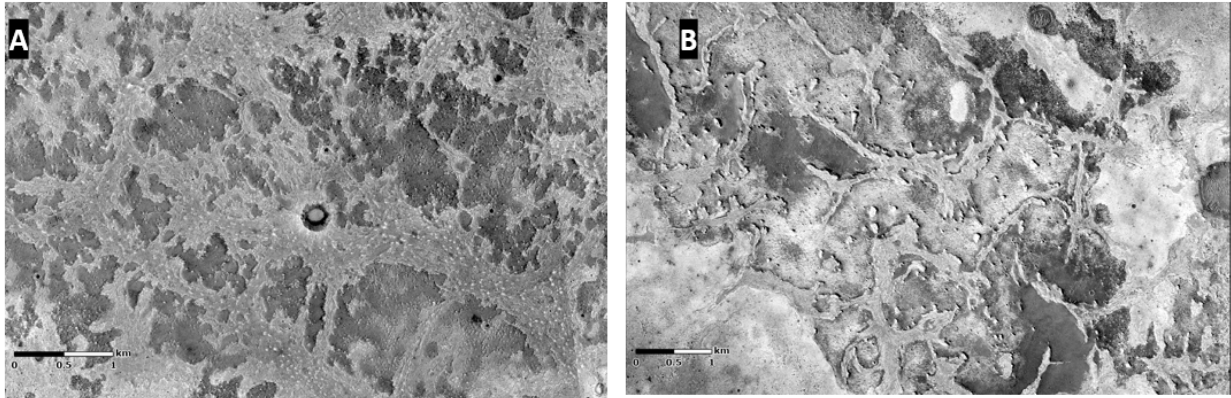


*Figure 13: Terrain Ridges in Region 1 UEU. (A) 5.95° E, 1.27° N (B) 2.86°E,0.09*

## C. In-Depth Look: Region 2

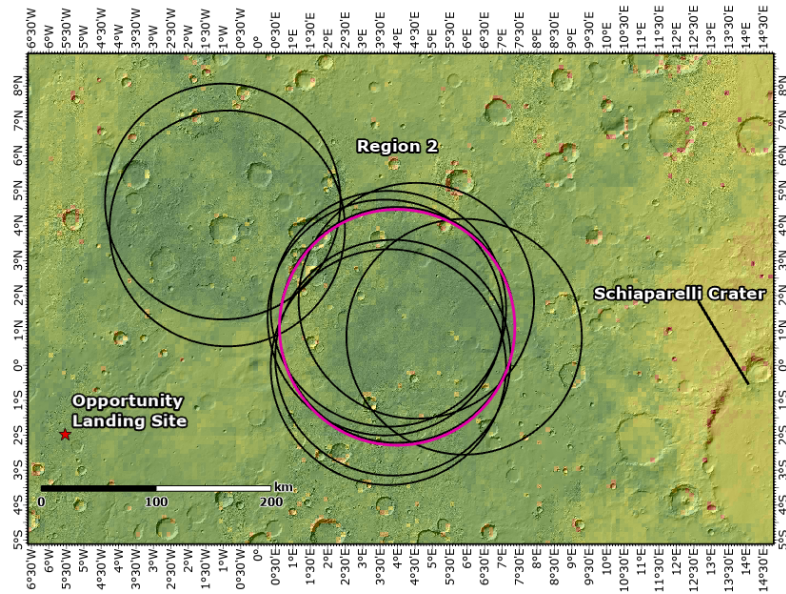


Figure 14: Region 2. Exploration zone 1539, with the highest suitability score, is colored in magenta. The final suitability raster, with transparency, is overlaying the MGS shaded relief map (Ferguson et al. 2017; own study).

Shown in Figure 14 is region 2, composed of a second set of 10 candidate exploration zones. While region 1 contains the 10 candidate exploration zones with the top 10 suitability scores, region 2 contains ranked sites 11-20 on the suitability scale. Much of region 2 and region 1 have overlap since the lower ranked candidate exploration zones in region 1 have similar suitability scores to the higher ranked candidate exploration zones in region 2.

Region 2 is very close to region 1, however, some of the exploration zones in region 2 sprawl slightly more to the north/north-west of Schiaparelli Crater than the more concentrated exploration zones of region 1. The center of the top ranked exploration zone in region 2, exploration zone 1539, is about 311 km away from the Opportunity landing site, a 14 km difference from the exploration zone 684 in region 1.

Table 3 shows exploration zone 1539 has the highest suitability score in region 2 at about 49.88 (medium-high suitability). Exploration zone 702 has the lowest suitability score in region 2 at 49.67( medium-high suitability). The zonal statistics analysis shows that the mean suitability between the exploration zones in region 2 are more similar than those in region 1, in fact, all of the exploration zones range between 49.5 and 49.9. Although region 2 has a slightly worse suitability score than region 1, their scores still fall in the medium-high suitability range.

It's worth noting that the difference between the highest and lowest candidate exploration zones in both regions is miniscule. However, this is expected because the candidate exploration zones are within the same larger area of eastern Sinus Meridiani. Also, the input dataset's resolution is relatively coarse--with higher resolution rasters there would be a greater opportunity to discern differences at the pixel scale.

Exploration Zone ID	Exploration Zone Rank	x (°)	y (°)	Suitability Score
700	13	3.87	0.24	49.83766
702	20	3.74	-0.03	49.67416
706	19	3.74	1.64	49.69684
768	14	-1.01001	4.71	49.82238
1177	18	-0.88	3.94	49.7282
1523	15	5.91	0.84	49.79212
1537	17	4.54	1.87	49.72886
1539	11	3.99	1.11	49.88105
1541	12	3.99	1.18	49.86495
1547	16	3.65	1.39	49.73016

*Table 3: Candidate exploration zones in region 2. Listed are the exploration zone coordinate in decimal degrees, exploration zone rank, suitability score and exploration zone ID.*

Like region 1, the two major units within region 2 are the SCU and UEU. However, there are areas of region 2 that also feature the Cratered Unit (CU) (orange colored in Figure 15) and

the Undivided Etched Unit (UEU2). The CU is known to form rough, cratered surfaces and generally feature high albedo and low thermal inertia (Hynek et al. 2017). Hynek et al. 2017 states that large impact craters, wrinkle ridges, scarps and troughs are found in this geologic unit.

The dark purple colored unit in Figure 15 is the UEU2 (Hynek et al. 2017). This unit features moderate albedo and thermal inertia value compared to other etched units (Hynek et al. 2017). The two candidate exploration zones in the grid north-west of region 2 also contain a Moderately Eroded Crater Unit (MECU), which indicates the craters have a relatively fresh central peak or ring structures (Hynek et al. 2017). The surrounding crater ejecta and secondary chains may still be preserved at this erosional state (Hynek et al. 2017). Furthermore, these craters may show evidence of infilling (Hynek et al. 2017)

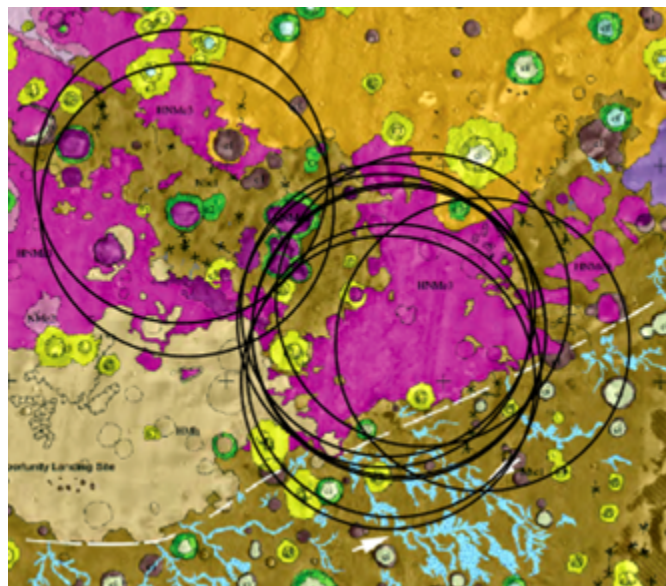


*Figure 15: Region 2 Geology. Overlain with the candidate exploration zones in region 2. Dark magenta color represents UEU, medium brown color represents the SCU, yellow is well-preserved crater unit, light blue color is internal crater deposit and dark purple is the undivided etched unit (UEU2). (Hynek et al. 2017 map edited by Wilkinson et al. 2023)*

Since 8 of the 10 candidate exploration zones in region 2 heavily overlap with most of region 1 the geology was quite similar. Candidate exploration zones 768 (rank 14) and 1177 (rank 18) are the most north-western of region 2 exploration zones and most obviously illustrate

the differences between the two regions. Exploration zones 768 and 1177 feature several massive craters ( greater than 20 km in diameter) that dominate much of the exploration zones.

Kozova crater , at the center of exploration zone 1177, is about 26 km in diameter and surrounded by a MECU (Figure 16), and is similar to most of the other large impact craters in these two exploration zones. The MECU surrounding Kozova features rugged terrain, ridges and younger impacts that have evidence of infilling.

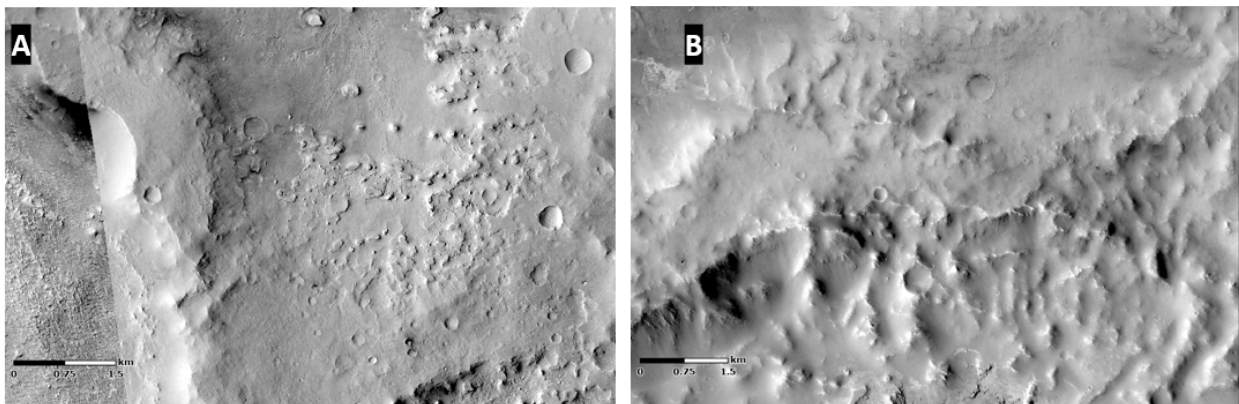


*Figure 16: Kozova Crater. (A) MECU around Kozova crater illustrating ridges, younger infilled craters and rugged terrain.  $.52^{\circ}W, 4.12^{\circ}N$  (B) MECU around Izamal crater illustrating rugged ridges and young infilled craters.  $1.57^{\circ}E, 4.25^{\circ}N$*

A prominent feature of candidate exploration zones 1177 and 768 is a crater complex in the east and south-east of the zones. The complex is comprised of Izamal crater (~26 km), Yelapa crater (~15km), and at least four additional unnamed craters over 8 km in diameter. Like Kozova crater, this complex is surrounded by a MECU also featuring rugged terrain, ridges, and small craters with evidence of infilling. There may be an opportunity to place a landing site in the relatively more benign SCU in EZ 1177 and 768. However, the increase in large crater population and more extensive ridge networks makes that task more difficult in comparison to the rest of region 2 and 1.

## **D. ICE-WG Requirements**

Based on exploration zone suitability and geology region 1 was chosen for landing site placement. While suitability and geology are certainly important factors to consider when placing a landing ellipse, they are not the sole deciding factors. Before finalizing the landing site and exploration zone, region 1 must also meet the requirements outlined by the ICE-WG and EMC in Bussey et al. (2016).

### **Requirement 1: Water-generating raw material**

The first exploration zone requirement is that the area demonstrates “ability to prospect for and extract useful commodities” (Bussey et al. 2016). The exploration zone must feature at least one location with access to significant quantities (>100 MT) of water that could be used for water-generating purposes such as hydrated minerals, ice or an ice/regolith mix (Bussey et al. 2016). When studying the SWIM dataset, it was found that region 1 exists in an area that indicates there may be the presence of ice at a depth of 0 - 1 m below the surface (Putzig et al. 2022).

Then, ESA’s hydrous mineral map was used to determine if there was evidence that region 1 hosted a concentration of hydrous mineral deposits since it is a listed resource that may be used for ISRU (Bussey et al. 2016). Figure 17 shows that region 1 features 120 instances of hydrous mineral deposits. Based on the SWIM and Hydrous Mineral deposit map region 1 meets requirement 1.

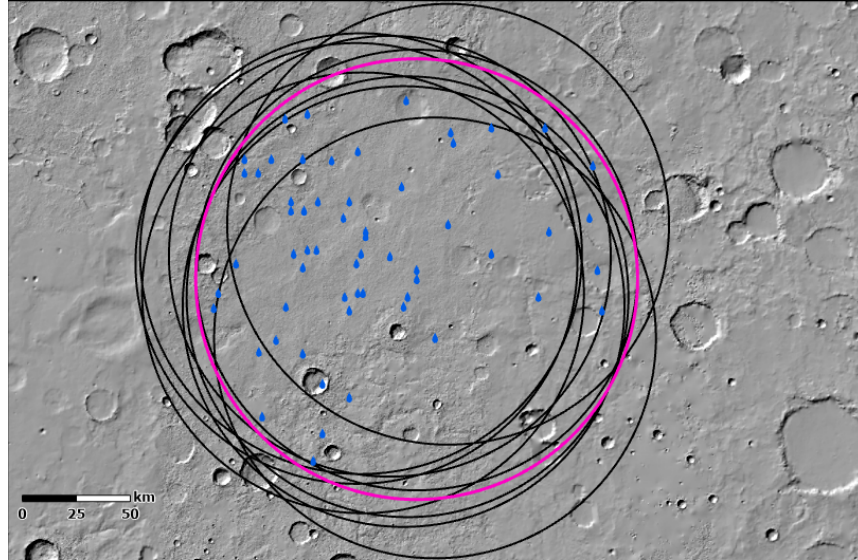


*Figure 17: Region 1 Hydrous Minerals. ESA's hydrous mineral detection (blue teardrop) map overlain region 1. Black circles are candidate exploration zones, magenta circle is the exploration zone 684 (highest suitability zone).*

## **Requirement 2: Construction Infrastructure**

Requirement 2 listed by ICE-WG in Bussey et al. (2016) states that the region must have access to an area that could host infrastructure for construction. Although ICE-WG does not specify the size of area needed for such infrastructure, the group does state that it must be within 5km from the central landing site (Bussey et al. 2016). Furthermore, there should be evidence for a significant (unspecified) amount of cobble-size stones, small rocks or bulk, loose regolith that would be used for construction techniques like leveling roadways or enhancing the surfaces of roads (Bussey et al. 2016).

While studying the geology of region 1, it was found that there were several landing site opportunities. For this requirement, these areas were re-visited and prospective construction sites were investigated. Edgett (2005) illustrates the types of geologic features found in Sinus Meridiani that may produce boulders and other rocky material that could either be broken down

or used outright for use in construction.

Edgett (2005) produced Figure 18 which illustrates that steep slopes and impact craters may produce boulders. For example, boulders can be found at the bottoms of cliffs and mesas (Edgett 2005). Furthermore, ejecta blankets are sometimes home to cobble sized material and boulders (Edgett 2005).

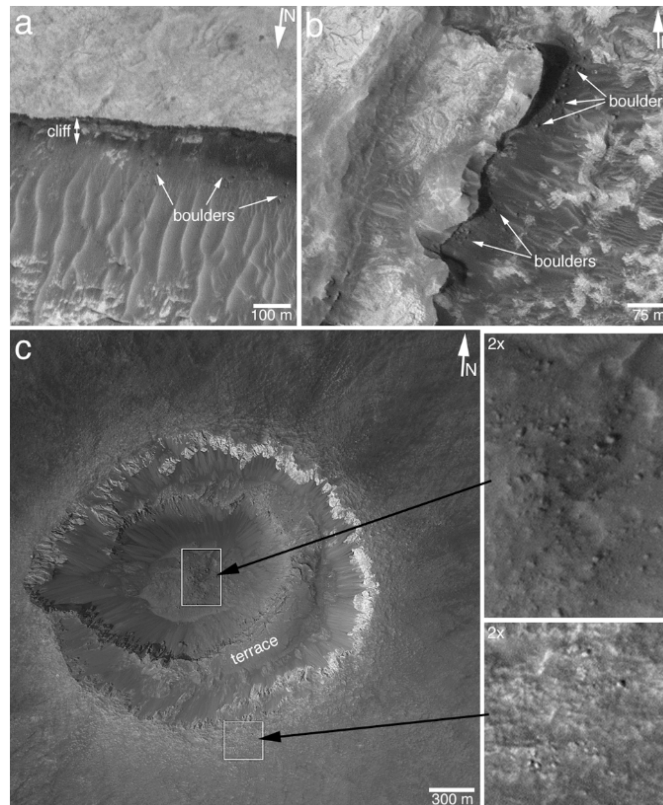


*Figure 18. Boulder Creating Geologic Features. Geologic features that may produce boulders like impact craters and steep slopes (Edgett 2005).*

Based on these examples it's likely that boulders and cobble sized material may be found all throughout region 1 (Figure 19). This is because there are many large impact craters scattered throughout the region, as well as scarps and cliffs where boulders and cobble-sized rocks and regolith could exist. Although Bussey et al. (2016) does not specify the need for boulders they may be even more useful for construction purposes than only cobble sized rocks since boulders can be broken down using hand tools or machinery and produce blocky material of different

sizes.

### **Requirement 3: Access to Metal or Silicon**

The TES Hematite mineral map shows Sinus Meridiani is one of the only two places on Mars where hematite was observed above the detection limit (Bandfield 2022). This area is west of region 1 near the Opportunity landing site. ICE-WG states the candidate exploration must have the *potential* to access a raw material that could be used as metal or silicon for both ISRU and construction (Bussey et al. 2016). The group specifies that their primary interests are iron, aluminum and silicon (Bussey et al. 2016). However, titanium and magnesium are also of interest, but not the priority (Bussey et al. 2016).

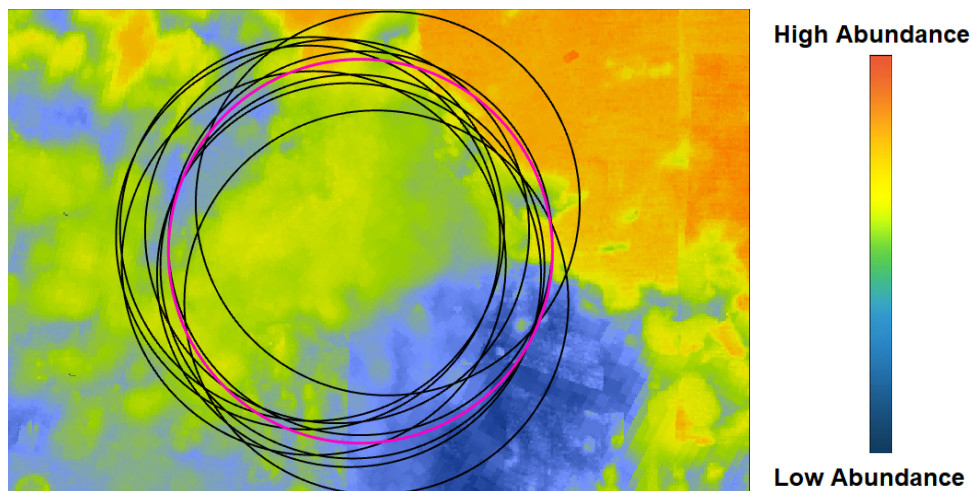


*Figure 19: Ferric Oxide in Region 1. Overlain ESA's ferric oxide mineral map. Right side shows how the color ramp correlates to abundance.*

Figure 20 illustrates the ferric oxide abundance according to OMEGA observations. Region 1 has a mixture of mid to low abundance of ferric oxide. The areas with the highest abundance of ferric oxide were deemed less suitable according to the suitability model because

their thermal inertia and albedo values did not align with the acceptable ranges outlined by Bussey et al. (2016). Based on these observations region 1 exhibits the potential to host a resource that could be used in the production of steel for manufacturing and therefore meets requirement 3.

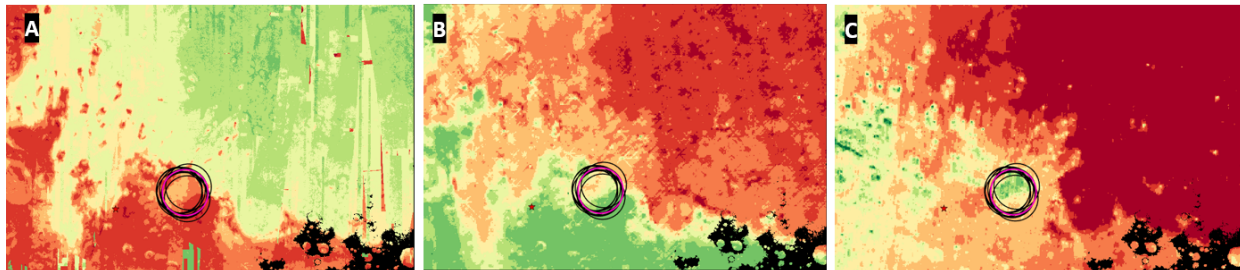


*Figure 20 illustrating why areas that have high abundances of ferric oxide are still less suitable over all. (A) Transformed ferric oxide raster. (B) Transformed albedo raster. (C) Transformed thermal inertia raster. Region 1 is overlain the rasters. Red colors are less suitable according to transformation scale, green colors are more suitable according to transformation scale.*

## **E. Proposed Landing Site**

A proposed landing site (LS) was placed in site region 1, within the SCU of candidate exploration zone 684, which also happens to be the most suitable candidate exploration zone according to the suitability model. Keeping in line with Bussey et al. (2016) recommendations, the landing site is an area of 25 km<sup>2</sup>, and located in an exploration zone of 200 km. Furthermore, the area meets the latitude requirement, altitude requirement and slope (according to MOLA data).

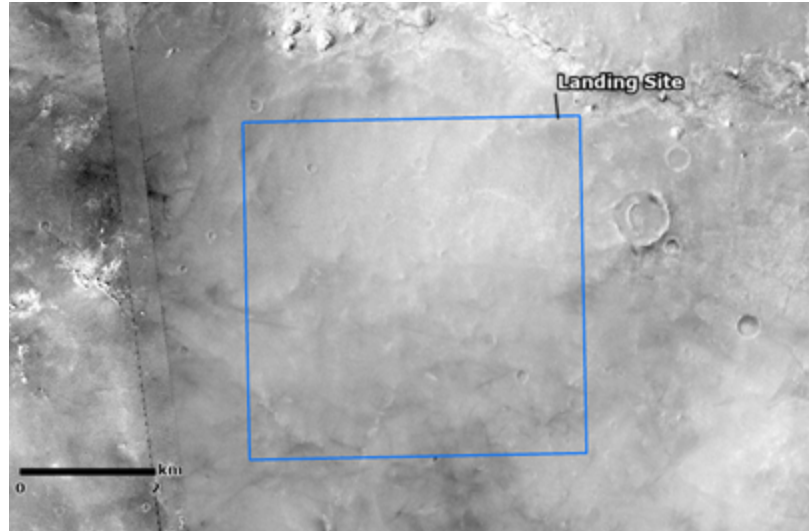


*Figure 21. Proposed Region 1 Landing Site.*

Bussey et al. (2016) specified the landing site should be significantly devoid of surface hazards like large/clustered craters (no maximum diameter given), mountainous terrain, chaotic terrain and extensive dune fields. Upon inspection of four different CTX frames, it's shown that there are a few hazards in the area, but the features aren't so severe that they affect the overall quality of the landing site. For example, as seen in Figure 21, there are a few craters in the 25 km<sup>2</sup> area. However, the craters aren't very large compared to others in the area, they aren't clustered, nor prominent, and appear to have experienced infilling.

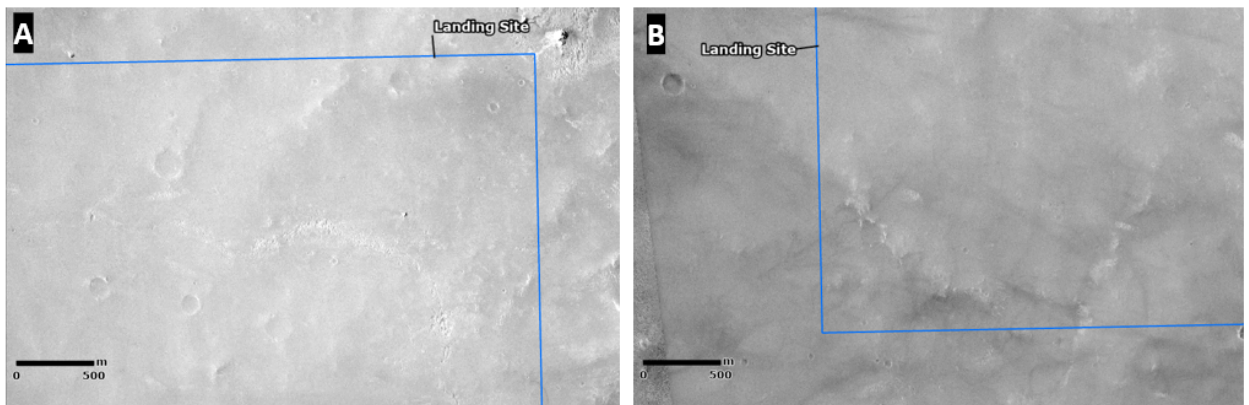


*Figure 22: Landing Site Geologic Features. (A) Grid north east of the landing site illustrating the crater population and ridge-type figure. (B) Grid south west corner of the landing site where a small ridge crosscuts the corner.*

In the grid north east, shown in Figure 22, there appears to be evidence of a ridge forming, however, the feature does not appear prominent nor extremely rugged in imagery. Furthermore, Figure 22 also shows that there is a small ridge cross cutting the corner of the landing site. Although the landing site does have a few hazards, they aren't so prominent that they obstruct or dominate the landing site area. Furthermore, Bussey et al. (2016) does not state that there must not be *any* hazards, rather implies the landing site must not be overwhelmed by surface hazards.

When placing the landing site special attention was given to analyzing the transformed albedo and thermal inertia values, since those datasets give insight into the area's dust cover, which is a potential hazard. Bussey et al. (2016) state that the area should not have thick deposits of dust. For example the site should not feature "extremely low" thermal inertia values and high albedo (Bussey et al. 2016).

Ruff et al. (2016) states that regions with an albedo value of less than .10 tend to correlate to dust-free locations. The transformed albedo raster (Figure 23) illustrates the landing site's albedo levels are straddling the first highest and second highest suitability values. A point inspection of the site shows that about a quarter of the landing site meets the less than .10 threshold. The rest of the landing site has a suitability score of 7 which equals an albedo range of .14 to .16.

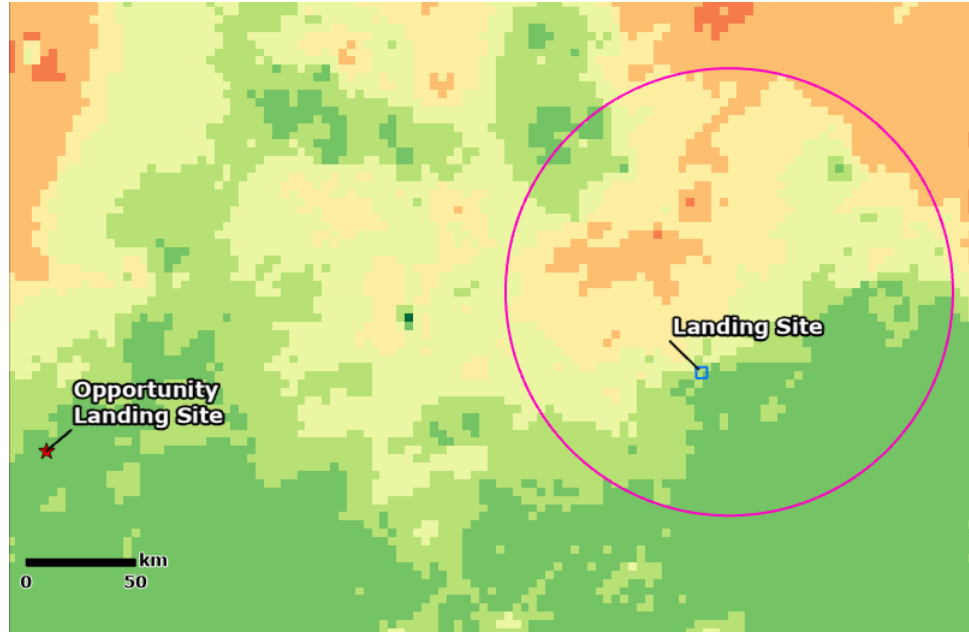


*Figure 23: Landing Site Albedo. Transformed albedo raster map showing that the landing site (blue square) is in an area where the albedo values meet hazard requirements. For comparison, Opportunity landing site (red star) albedo is also shown..*

Since the coarse resolution of this dataset may not be offering the level of granularity needed to discern incremental changes of albedo values over the entire landing site, it could be that the region is dust-free in terms of albedo or have light coverage which does not lead one to believe this area has thick dust deposits.

For comparison, a point inspection was done on the transformed albedo raster where Opportunity landed (Figure 23). Since this was a successful landing, it's useful to compare metrics between landing sites when they are in close proximity. The transformed albedo raster shows that the Opportunity landing site has an albedo suitability score of 8 in a range of 0.1 to 0.14. This shows that in regards to albedo LS and the Opportunity landing site have similar albedo characteristics.

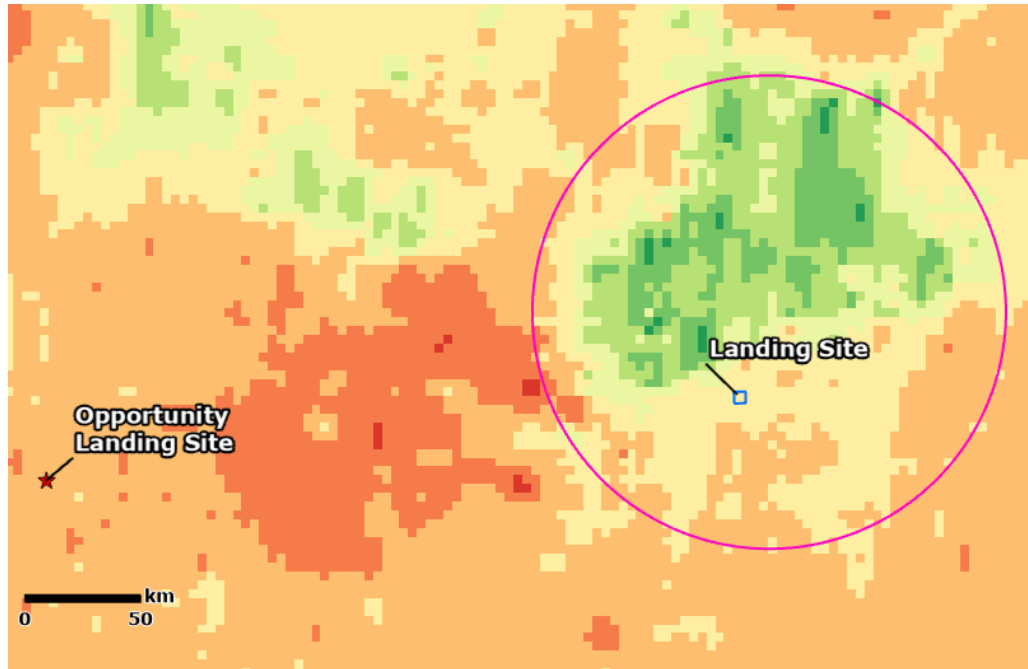


*Figure 24: Landing Site Thermal Inertia. Transformed thermal inertia map showing that the landing site (blue square) is an area where the thermal inertia values meet hazard requirements.*

When inspecting the transformed thermal inertia values, the landing site is an area that would be considered “moderate suitability.” According to the transformation plot, the proposed landing site is in a thermal inertia range of 250-300 IU. Unacceptable thermal inertia values were identified by Ruff et al. as less than 100 IU (2016), therefore, these values are acceptable in regards to hazard mitigation. Again, for comparison, Figure 24 illustrates that the Opportunity landing site has slightly less suitable thermal inertia than the landing site in region 1. The Opportunity landing site has a suitability score of 4, which correlates to a range of 150-200 IU.

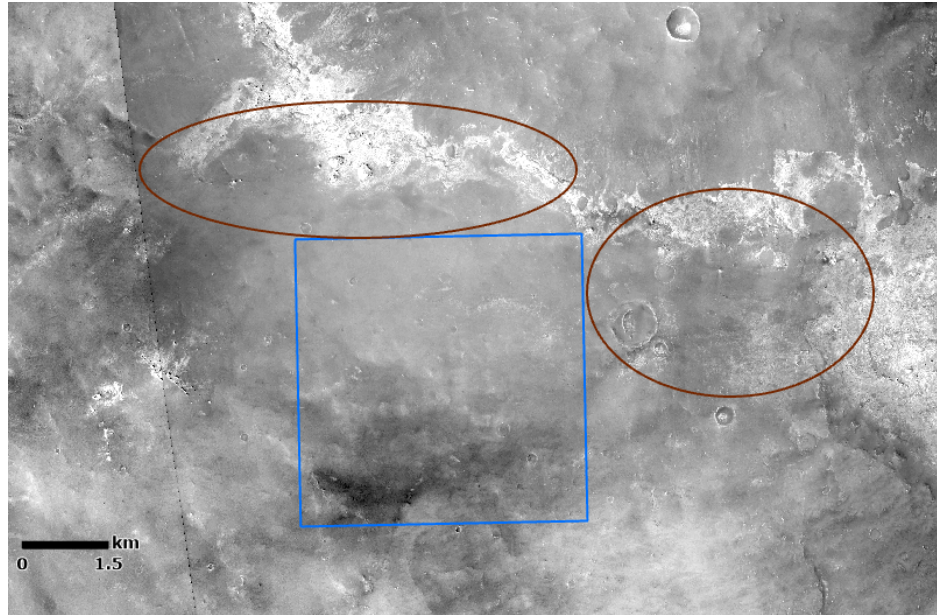


*Figure 25. Landing Site Construction Potential. This illustrates that the proposed landing site (blue box) is near a scarp to the north that could be used for construction where blocks or cobble sized material could be found at the base for construction.*

Regarding ICE-WG requirement 2 stating there must be an area within 5 km of the landing site that could be used for construction purposes, Figure 25 shows two such areas (brown ellipses). These areas appear to have flat, stable terrain and are in proximity to the base of a scarp. The scarp could have cobble sized material or boulders at its base that could be broken down using machinery or hand tools.

## V. CONCLUSIONS

In conclusion, my findings show that the Sinus Meridiani area of Mars is most suitable in terms of the ICE-WG parameters listed in Bussey et al. (2016). A candidate landing zone (EZ 684) was selected in one of the Sinus Meridiani sub regions (referred to as region 1). This exploration zone meets the base requirements listed by Bussey et al. including being located between +/- 50° latitude, is less than + 2 km in elevation and, does not have thick deposits of dust, and features an area of 25 km<sup>2</sup> that is generally level and devoid of hazards.

Furthermore the exploration zone meets all 3 requirements identified by ICE-WG that were developed to pursue NASA's goal of a permanent and sustainable Maritan presence. Candidate exploration zone 684 meets requirement 1 since ESA hydrous mineral deposit map shows that there are many instances of hydrous mineral deposits. Also, SWIM data indicates there may be the presence of water-ice 0-1 m below the surface. Requirement 2 is met as seen in Figure 25 where two construction infrastructure areas are identified. Lastly, requirement 3 is met as ESA's ferric oxide map shows there appears to be a moderate abundance of ferric oxide, a mineral used in the production of steel (Garrison 2001).

A landing site (Figure 21) is proposed in exploration zone 684 that is 25 km<sup>2</sup> and meets all the base requirements listed by Bussey et al. (2016). In addition, the landing site is generally devoid of all major hazards, but not completely hazard free. The landing site contains several relatively small craters with evidence of infilling. Also, there are two ridges near the corners of the square landing site that would be hazardous for a landing. However, from visual analysis of four CTX images, the vast majority of the 25 km<sup>2</sup> is flat, stable and does not contain other hazards like large boulders. Furthermore, upon inspection of the transformed albedo and thermal inertia values, the landing site is dust free, which is another listed hazard (Bussey et al. 2016).

As future data collection missions occur, there will be an increase in the quantity, quality and diversity of available datasets. This will lead to future work where more precise location suitability analysis can be completed. New data that would benefit this effort includes higher spatial resolution DEMs, higher resolution surface characteristic data (ex. albedo, thermal inertia) and more accessible resource maps.

A note on having more accessible resource maps, this plays into the fact that the author found it difficult to address some of the key requirements in regards to resources. Specifically, the parts of the requirements that stated a certain quantity of said resource should be available within an exploration zone. At the time of this project, there were not many publicly available resources that the author found that helped non-expert persons understand how to measure resource quantities from remote sensing data sets like ESA's ferric oxide map.

In the future, the author would like to consult more subject matter experts, particularly in the fields of geochemistry and mineralogy. This would give more insights into the type of datasets that could be ingested in the suitability model that could improve the accuracy of the model.

Furthermore, the author would revisit this project if additional workshops similar to the "First Landing Site/Exploration Zone Workshop for Human Missions to the Surface of Mars" were announced. This is because it's assumed another workshop of this kind would include updated exploration zone requirements that are more reflective of current goals.

## REFERENCES

- Ahmad, Adnan, and Archana M Nair. "Landform Evolution of Tharsis Montes and Olympus Mons of Mars: Insights from Morphometric, Hypsometric and Chronologic Evidences." *Journal of Earth System Science* 130, no. 3 (2021). <https://doi.org/10.1007/s12040-021-01672-5>.
- Barker, Michael. MOLA. Accessed November 9, 2023. <https://tharsis.gsfc.nasa.gov/MOLA/mola.php>.
- Barlow, Nadine G. *Mars an introduction to its interior, surface and atmosphere*. Cambridge: Cambridge University Press, 2014.
- Bobskill, Marianne R., Mark L. Lupisella, Rob P. Mueller, Laurent Sibille, Scott Vangen, and Julie Williams-Byrd. "Preparing for Mars: Evolvable Mars Campaign &#X201C;Proving Ground&#X201D; Approach." *2015 IEEE Aerospace Conference*, 2015. <https://doi.org/10.1109/aero.2015.7119274>.
- Bussey, Ben, and Stephen J Hoffman. Rep. *Human Mars Landing Site and Impacts of Mars Surface Operations*, 2016.
- Carter, J., F. Poulet, J.-P. Bibring, N. Mangold, and S. Murchie. "Hydrous Minerals on Mars as Seen by the CRISM and Omega Imaging Spectrometers: Updated Global View." *Journal of Geophysical Research: Planets* 118, no. 4 (2013): 831–58. <https://doi.org/10.1029/2012je004145>.
- Christensen, P. R., J. L. Bandfield, V. E. Hamilton, S. W. Ruff, H. H. Kieffer, T. N. Titus, M. C. Malin, et al. "Mars Global Surveyor Thermal Emission Spectrometer Experiment: Investigation Description and Surface Science Results." *Journal of Geophysical Research: Planets* 106, no. E10 (2001): 23823–71. <https://doi.org/10.1029/2000je001370>.
- Christensen, Philip R. "Global Albedo Variations on Mars: Implications for Active Aeolian Transport, Deposition, and Erosion." *Journal of Geophysical Research: Solid Earth* 93, no. B7 (1988): 7611–24. <https://doi.org/10.1029/jb093ib07p07611>.
- Edgett, Kenneth S. "The Sedimentary Rocks of Sinus Meridiani: Five Key Observations from Data Acquired by the Mars Global Surveyor and Mars Odyssey Orbiters." *The Mars Journal*, 2005, 5–58. <https://doi.org/10.1555/mars.2005.0002>.
- Ferguson, R. L., T. M. Hare, and J. Laura. "Mars MGS MOLA - MEX HRSC Blended Shaded Relief 200m V2." Map. Astrogeology PDS Annex, U.S. Geological Survey, 2017.

- Garrison, W. M. “Ferrous Alloys: Overview.” Essay. In *Encyclopedia of Materials: Science and Technology*, edited by H I Aaronson, 2nd ed. Elsevier Ltd., 2001.
- “The General Suitability Modeling Workflow.” The general suitability modeling workflow-ArcGIS Pro | Documentation, 2023.  
<https://pro.arcgis.com/en/pro-app/latest/help/analysis/spatial-analyst/suitability-modeler/the-general-suitability-modeling-workflow.htm>.
- Hartmann, William K. *A Traveler’s Guide to Mars*. Toronto: Thomas Allen & Son, 2003.
- Hoffman, Stephen J. “Evolvable Mars Campaign Development.” Smithsonian’s S. Dillon Ripley Center, May 24, 2016.
- Hynek, Brian, and Gaetano Di Achille. “Geologic Map of Meridiani Planum, Mars.” Map. U.S. Geological Survey Scientific Investigations Map, 2017.
- “Introduction to the Suitability Modeler.” Introduction to the Suitability Modeler-ArcGIS Pro | Documentation, 2023.  
<https://pro.arcgis.com/en/pro-app/latest/help/analysis/spatial-analyst/suitability-modeler/what-is-the-suitability-modeler.htm>.
- “ISIS- Integrated Software for Imagers and Spectrometers.” USGS Isis: Planetary Image Processing Software, 2022. <https://isis.astrogeology.usgs.gov/7.0.0/index.html>.
- Jakosky, Bruce, Richard Zurek, Shane Byrne, Wendy Calvin, Behthany Ehlmann, and Shannon Curry. Rep. *Mars, the Nearest Habitable World—A Comprehensive Program for Future Mars Exploration*. Mars Architecture Strategy Working Group (MASWG), 2020.  
<https://mepag.jpl.nasa.gov/reports/MASWG%20NASA%20Final%20Report%202020.pdf>.
- Jaumann, R., G. Neukum, T. Behnke, T.C. Duxbury, K. Eichentopf, J. Flohrer, S.v. Gasselt, et al. “The High-Resolution Stereo Camera (HRSC) Experiment on Mars Express: Instrument Aspects and Experiment Conduct from Interplanetary Cruise through the Nominal Mission.” *Planetary and Space Science* 55, no. 7–8 (2007): 928–52.  
<https://doi.org/10.1016/j.pss.2006.12.003>.
- Kirkby, Kent. “Hematite.” Hematite | Common Minerals. Accessed November 29, 2023.  
<https://commonminerals.esci.umn.edu/minerals-g-m/hematite>.
- Komatsu, G., T. Ruj, H. Miyamoto, J. M. Dohm, J. Ormo, and K. Kurosawa. “Lunar and Planetary Science XLVIII .” In *THE HELLAS BASIN ON MARS: FURTHER EXPLORATION OF ITS ANOMALOUS SHAPE*. Woodlands, TX, n.d.
- Kuziakina, Marina, Dmitry Gura, and Dmitry Zverok. “GIS Analysis of Promising Landing Sites for Manned Flight to Mars.” *E3S Web of Conferences* 138 (2019): 02004.  
<https://doi.org/10.1051/e3sconf/201913802004>.

- Kuźma, Marta, Łukasz Gładysz, Mateusz Gralewicz, and Paweł Krawczyk. “Applications of GIS in Analysis of Mars.” *Lecture Notes in Geoinformation and Cartography*, 2017, 267–76. [https://doi.org/10.1007/978-3-319-61297-3\\_19](https://doi.org/10.1007/978-3-319-61297-3_19).
- Malin, Michael. “Mars Reconnaissance Orbiter (MRO) Context Camera (CTX).” Malin Space Science Systems - Mars Reconnaissance Orbiter (MRO) Context Camera (CTX), 2023. [https://www.msss.com/all\\_projects/mro-ctx.php](https://www.msss.com/all_projects/mro-ctx.php).
- “Mars Exploration Rovers.” NASA. Accessed November 8, 2023. <https://mars.nasa.gov/mer/>.
- “Mars Express Overview.” Mars Express overview. Accessed November 9, 2023. [https://www.esa.int/Science\\_Exploration/Space\\_Science/Mars\\_Express\\_overview](https://www.esa.int/Science_Exploration/Space_Science/Mars_Express_overview).
- “Mars Ferric Oxide Map.” Mars ferric oxide map, September 2019. [https://www.esa.int/ESA\\_Multimedia/Images/2013/05/Mars\\_ferric\\_oxide\\_map](https://www.esa.int/ESA_Multimedia/Images/2013/05/Mars_ferric_oxide_map).
- Morgan, G. A., N. E. Putzig, M. R. Perry, H. G. Sizemore, A. M. Bramson, E. I. Petersen, Z. M. Bain, et al. “Availability of Subsurface Water-Ice Resources in the Northern Mid-Latitudes of Mars.” *Nature Astronomy* 5, no. 3 (2021): 230–36. <https://doi.org/10.1038/s41550-020-01290-z>.
- Ody, A., F. Poulet, Y. Langevin, J.-P. Bibring, G. Bellucci, F. Altieri, B. Gondet, M. Vincendon, J. Carter, and N. Manaud. “Global Maps of Anhydrous Minerals at the Surface of Mars from Omega/Mex.” *Journal of Geophysical Research: Planets* 117, no. E11 (2012). <https://doi.org/10.1029/2012je004117>.
- Pajola, Maurizio, Sandro Rossato, Emanuele Baratti, and Alexandre Kling. “Planetary Mapping for Landing Sites Selection: The Mars Case Study.” *Lecture Notes in Geoinformation and Cartography*, 2019, 175–90. [https://doi.org/10.1007/978-3-319-62849-3\\_7](https://doi.org/10.1007/978-3-319-62849-3_7).
- Presley, Marsha A., and Philip R. Christensen. “Thermal Conductivity Measurements of Particulate Materials: 5. Effect of Bulk Density and Particle Shape.” *Journal of Geophysical Research: Planets* 115, no. E7 (2010). <https://doi.org/10.1029/2009je003483>.
- Putzig, Nathaniel, and Gareth A Morgan. “53rd Lunar and Planetary Science Conference.” In *Subsurface Water Ice Mapping (SWIM) to Support the International Mars Ice Mapper (I-MIM) Mission*. Woodlands, Texas, 2022.
- Rodriguez, J. Alexis, Eldar Noe Dobrea, Jeffrey S. Kargel, V. R. Baker, David A. Crown, Kevin D. Webster, Daniel C. Berman, Mary Beth Wilhelm, and Denise Buckner. “The Oldest Highlands of Mars May Be Massive Dust Fallout Deposits.” *Scientific Reports* 10, no. 1 (2020). <https://doi.org/10.1038/s41598-020-64676-z>.

- Rouault, Even, Frank Warmerdam, Kurt Schwehr, Andrew Kiselev, and Howard Butler. Computer software. *GDAL*, 2023. <https://gdal.org/#>.
- Ruff, Steven W., and Philip R. Christensen. “Bright and Dark Regions on Mars: Particle Size and Mineralogical Characteristics Based on Thermal Emission Spectrometer Data.” *Journal of Geophysical Research: Planets* 107, no. E12 (2002). <https://doi.org/10.1029/2001je001580>.
- Senate - Commerce, Science, and Transportation, and John D Rockefeller, National Aeronautics and Space Administration Authorization Act of 2010 § (2010).
- Senate Appropriations, and Tim Ryan. Bill, Chips and Science Act of 2022 § (2021).
- “Slope (Spatial Analyst).” Slope (Spatial Analyst)-ArcGIS Pro | Documentation. Accessed November 9, 2023. <https://pro.arcgis.com/en/pro-app/latest/tool-reference/spatial-analyst/slope.htm>.
- Smith, David E., Maria T. Zuber, Herbert V. Frey, James B. Garvin, James W. Head, Duane O. Muhleman, Gordon H. Pettengill, et al. “Mars Orbiter Laser Altimeter: Experiment Summary after the First Year of Global Mapping of Mars.” *Journal of Geophysical Research: Planets* 106, no. E10 (2001): 23689–722. <https://doi.org/10.1029/2000je001364>.
- Smith, David E., Maria T. Zuber, Sean C. Solomon, Roger J. Phillips, James W. Head, James B. Garvin, W. Bruce Banerdt, et al. “The Global Topography of Mars and Implications for Surface Evolution.” *Science* 284, no. 5419 (1999): 1495–1503. <https://doi.org/10.1126/science.284.5419.1495>.
- Tanaka, Kenneth L., James A. Skinner, and Trent M. Hare. Map. *Geologic Map of the Northern Plains of Mars*. Reston, Va.? U.S. Geological Survey, 2005.
- Warmerdam, Frank. “The Geospatial Data Abstraction Library.” *Open Source Approaches in Spatial Data Handling*, n.d., 87–104. [https://doi.org/10.1007/978-3-540-74831-1\\_5](https://doi.org/10.1007/978-3-540-74831-1_5).
- Watters, Thomas R., Patrick J. McGovern, and Rossman P. Irwin III. “Hemispheres Apart: The Crustal Dichotomy on Mars.” *Annual Review of Earth and Planetary Sciences* 35, no. 1 (2007): 621–52. <https://doi.org/10.1146/annurev.earth.35.031306.140220>.
- Werner, S.C., K.L. Tanaka, and J.A. Skinner. “Mars: The Evolutionary History of the Northern Lowlands Based on Crater Counting and Geologic Mapping.” *Planetary and Space Science* 59, no. 11–12 (2011): 1143–65. <https://doi.org/10.1016/j.pss.2011.03.022>.
- Wilkinson, M. Justin, and Ricardo Vilalta. “Megafans on Mars A Fluvial Analogue for the Sinus Meridiani Layered Sediments.” Essay. In *Fluvial Megafans on Earth and Mars*, edited by Mark Salvatore. Cambridge University Press & Assessment, 2023.

Williams, Greg, and Jason Crusan. "National Aeronautics and Space Administration  
Pioneering Space – the Evolvable Mars Campaign," April 2015